DETERMINATION OF THE CRITICAL DRAWDOWN PRESSURE TO PREDICT POTENTIAL RISK OF SAND PRODUCTION OF A GAS WELL IN BANGLADESH

Md. Kaoser Hasan

DEPARTMENT OF PETROLEUM & MINERAL RESOURCES ENGINEERING

BUET, DHAKA, BANGLADESH

JUNE 2016

DETERMINATION OF THE CRITICAL DRAWDOWN PRESSURE TO PREDICT POTENTIAL RISK OF SAND PRODUCTION OF A GAS WELL IN BANGLADESH

A Project

Submitted to the Department of Petroleum & Mineral Resources Engineering

in partial fulfillment of the requirements for the

Degree of Master of Engineering (Petroleum)

By

Md. Kaoser Hasan

DEPARTMENT OF PETROLEUM & MINERAL RESOURCES ENGINEERING

BUET, DHAKA, BANGLADESH

JUNE 2016

CANDIDATE'S DECLARATION

It is hereby declared that this project or any part of it has not been submitted elsewhere for the award of any degree or diploma.

Signature of the Candidate

K. Hasan.

....

(Md. Kaoser Hasan)

RECOMMENDATION OF THE BOARD OF EXAMINERS

The undersigned certify that they have read and recommended to the department of Petroleum and Mineral Resources Engineering, for acceptance, a project entitled "DETERMINATION OF THE CRITICAL DRAWDOWN PRESSURE TO PREDICT POTENTIAL RISK OF SAND PRODUCTION OF A GAS WELL IN BANGLADESH" submitted by Md. Kaoser Hasan in partial fulfillment of the requirements for the degree of MASTER OF ENGINEERING in PETROLEUM ENGINEERING.

Chairman (Supervisor): ______________________

Shahriar Mahmud
Assistant Professor,
Dept. of Petroleum & Mineral Resources Engineering,
BUET

Member : ______________________

Dr. Mohammed Mahbubur Rahman
Associate
Professor,
Dept. of Petroleum & Mineral Resources Engineering,
BUET

Member : ______________________

Farhana Akter
Assistant Professor,
Dept. of Petroleum & Mineral Resources Engineering,
BUET

Date: 22-Jun-2016

ABSTRACT

Sub-surface formations are always in a stressed state, mostly due to overburden and tectonic stresses. When an oil or gas well is drilled into a formation, stressed solid material is removed. The fluid pressure of the borehole supports the borehole wall. As this fluid pressure generally does not match with the in situ formation stresses, there will be stress redistribution around the wellbore. The new stress may be greater than the stress that the formation can support and subsequently failure may occur. Knowledge of the stresses around a well is therefore imperative to determine the wellbore stability and subsequently any potential risk of sand production.

Due to lack of proper knowledge for calculating Critical Drawdown Pressure and predicting sand production, some gas wells in Bangladesh have started producing sand. For the same reason, production rate from some gas wells have been kept limited assuming that sand production may trigger although the well formation has sufficient strength to prevent sand production.

The main objective of this project is to determine the Critical Drawdown Pressure of a gas well which is the maximum difference between reservoir pressure and bottom-hole flowing pressure that the formation can withstand without sand being produced along with the formation fluid. Different existing Models have been used for this purpose and comparative analysis of those models have been performed. Based on this study, the Drucker-Prager model result meets and explain the current operating condition of the sample gas well. Hence with all its limitation, Drucker-Prager failure criterion has been considered a reliable criterion to predict sanding production when the well is in production.

ACKNOWLEDGEMENT

I would like to express my appreciation to those individuals who helped me to produce this work. First and foremost, my appreciation is extended to my project supervisor Shahriar Mahmud (Assistant Professor, PMRE, BUET) who has spent significant time guiding me and providing valuable suggestions towards completion of this work.

I am grateful to Dr. Mohammed Mahbubur Rahman (Associate Professor, PMRE, BUET) and Farhana Akter (Assistant Professor, PMRE, BUET) for their valuable time as the examiners of the report and their insightful ideas and suggestions.

NOMENCLATURE

Area	A	in^2
Stress	σ	psi
In-Situ Vertical or Overburden Stress	σ_V	psi
In-Situ Maximum Horizontal Stress	σ_H	psi
In-Situ Minimum Horizontal Stress	σ_h	psi
Major Principal Stress	σ_1	psi
Intermediate Principal Stress	σ_2	psi
Minor Principal Stress	σ_3	psi
Effective Major Principal Stress	σ_1'	psi
Effective Intermediate Principal Stress	σ_2'	psi
Effective Minor Principal Stress	σ_3'	psi
In-Situ Normal Stresses in Wellbore Coordinate System	$\sigma_x, \sigma_y, \sigma_{zz}$	psi
In-Situ Shear Stresses in Wellbore Coordinate System	$\tau_{xy}, \tau_{yz}, \tau_{zx}$	psi
Radial Stress at the wellbore wall	σ_r	psi
Hoop Stress at the wellbore wall	σ_θ	psi
Axial Stress at the wellbore wall	σ_z	psi
Shear Stresses at the wellbore wall	$\tau_{\theta z}, \tau_{r\theta}, \tau_{zr}$	psi
Hole or Well Deviation from vertical	α	degree
Mohr-Coulomb Angle of Internal Friction	ϕ	degree
Angular position around Wellbore Circumference	ϴ	degree
Wellbore Azimuth	ɣ	degree
Angle between the hole direction (projection on plane) and σ_H direction (counterclockwise positive from σ_H direction)	β	degree
Direction of Min. Horizontal stress with Azimuth	$ɣ_h$	degree
Direction of Max. Horizontal stress with Azimuth	$ɣ_H$	degree
Reservoir Depth	H	feet
Reservoir Pore pressure at the wellbore wall	P_f	psi

Far Field Pore pressure	P_F	psi
Wellbore Pressure	P_w	psi
Wellbore Minimum Pressure	$P_{w,Min}$	psi
Critical Drawdown Pressure	P_{CD}	psi
Poisson Ratio	ν	
Biot's Poroelastic Constant	k	
Cohesion or Cohesive Shear Strength	S_o	psi
Material Constant (Ewy Modified Lade Failure Criterion)	S_1	psi
Material Constant (Ewy Modified Lade Failure Criterion)	η	
Modified Lade First Stress Invariant	$I_1^{"}$	psi
Modified Lade Third Stress Invariant	$I_3^{"}$	psi^3
Material Constant (Mogi-Coulomb Failure Criterion)	a	
Material Constant (Mogi-Coulomb Failure Criterion)	b	
Effective Mean Stress	$\sigma'_{m,2}$	psi
Octahedral Shear Stress	τ_{oct}	psi
Material Constant (Drucker-Prager Failure Criterion)	a	
Material Constant (Drucker-Prager Failure Criterion)	k	psi
First Stress Invariant	I_1	psi
Second Deviatroric Stress Invariant	J_2	psi

Table of Contents

Abstract v

Acknowledgment vi

Nomenclature vii

Chapter 1: Introduction 5

1.1. Objectives 6

Chapter 2: Literature Review 7

2.1. Rock Mechanics 7

2.1.1. Stress 7

2.1.2. Stress Tensor 9

2.1.3. Principal Stresses in Two Dimensions 10

2.1.4. In-Situ Stress 11

2.1.5. Wellbore Stresses in Rectangular Coordinate System 13

2.1.6. Wellbore Stresses in Polar Coordinate System 14

2.1.7. Effective Stress Concept 17

2.1.8. Critical Drawdown Pressure 18

2.2. Type of Formation Rock Failure 18

2.2.1. Tensile Failure 19

2.2.2. Shear Failure 19

2.2.3. Compaction Failure 20

2.3. Formation Rock Failure Criterion 21

2.3.1. Mohr-Coulomb failure criterion 21

2.3.2. Drucker-Prager failure criterion 25

2.3.3. Mogi-Coulomb failure criterion 26

2.3.4. Ewy Modified Lade Failure criterion 27

2.4. Formation Mechanical Properties and Stress Data Acquisition 28

2.4.1. Laboratory Core Tests 29

2.4.2. Measurement While Drilling 31

2.4.3. Wireline Logging Methods 34

Chapter 3: Outlined Methodology 39

3.1. Mohr-Coulomb Failure Criterion 40

3.2. Ewy Modified Lade Failure Criterion 40

3.3. Mogi-Coulomb Failure Criterion 41

3.4. Drucker-Prager Failure Criterion 41

Chapter 4: Case Study 43

4.1.1. Critical Drawdown Pressure Calculation 45

4.1.2. CDP Calculation by Calculation Mohr-Coulomb Failure Criterion..........49
4.1.3. CDP Calculation by Modified Lade Criterion..51
4.1.4. CDP Calculation by Mogi-Coulomb Failure Criterion.............................52
4.1.5. CDP Calculation by Drucker-Prager Failure Criterion.............................53

Chapter 5: Observations and Discussions ……………………………………………….. 54

Chapter 6: Conclusions and Recommendations ………………………………………. 57

References …………………………………………………………………………... 59
Appendix - A...61
Stresses around Wellbore #A calculation (Step 2 – 4) 61
Appendix - B...63
CDP calculation by Mohr-Coulomb Failure Criterion 63
Appendix - C 66
CDP calculation by Modified Lade Failure Criterion..66
Appendix - D 70
CDP calculation by Mogi-Coulomb Failure Criterion...70
Appendix - E...74
CDP calculation by Drucker-Prager Failure Criterion...74

LIST OF FIGURES

Figure 2-1: Illustration of forces and stress 8

Figure 2-2: Decomposition of forces 8

Figure 2-3: Component of Stress 9

Figure 2-4: Force equilibrium on a triangle. 10

Figure 2-5: In-Situ Stresses...11

Figure 2-6: Defining Stresses in the In-Situ and Rectangular Wellbore Coordinate Systems 14

Figure 2-7: Wellbore Stresses in the Polar Coordinate System 15

Figure 2-8: Stress State at the Wall of a Deviate Wellbore 15

Figure 2-9: Tensile Failure...19

Figure 2-10: Shear Failure 19

Figure 2-11: Grain reorientation resulting in a closer packing 20

Figure 2-12: Location of the various failure modes in principal stress space 21

Figure 2-13: Failure line in the Shera Stress-Normal Stress Diagram...............................22

Figure 2-14: Mohr-Coulomb failure model from Triaxial test data 23

Figure 2-15: Ultimate Axial Stress-Confining Pressure Curve 24

Figure 2-16: Mohr–Coulomb criterion in τ–σ’ space with Mohr’s circle corresponding to a critical stress state. 24

Figure 2-17: Illustration of Core Testing 29

Figure 2-18: Schematic drawing of Tri-axial Test Cell (Fjaer et.al. 2008. P. 265) 30

Figure 2-19: Sample of Hole Collapse Test (Ewy et. al. 1990) 31

Figure 2-20: Extended Leak-Off Test showing pressure as a function of volume 33

Figure 2-21: Principal Sketch of a full waveform sonic tool...35

Figure 2-22: Illustration of directions for compressive and tensile failure around a vertical borehole..37

Figure 2-23: A resistivity Image Log of a North Sea Well..38

Figure 4-1: Ultimate Axial Stress-Confining Pressure Curve for Well #A.......................46

Figure 4-2:Mohr-Coulomb Criterion in τ-σ/ space for Well #A.......................................47

Figure 4-3: Wellbore and Wellbore Minimum/Maximum Stress Azimuth.......................48

Figure 4-4: Mohr-Coulomb Circle for Well #A with Failure Envelope............................50

LIST OF TABLES

Table 4-1: Reservoir and Production Information...43

Table 4-2: Well information 44

Table 4-3: Wellbore Stress Information 44

Table 4-4: Core Sample Information..45

Table 4-5: Triaxial Test Data for Well #A core...45

Table 4-6: In-Situ Stresses at the wellbore wall 47

Table 4-7: Stresses in Rectangular Wellbore Coordinate System 48

Table 4-8: Mohr-Coulomb Failure Criterion Calculation..49

Table 4-9: Modified Lade Failure Criterion Calculation...51

Table 4-10: Mogi-Coulomb Failure Criterion Calculation..52

Table 4-11: Drucker-Prager Failure Criterion Calculation..53

Table 4-12: Summary Result Sanding Potentiality Evaluation of Well #A 54

Chapter 1: Introduction

Sand production during hydrocarbon production is a major economic and technical issue. On one hand, unnecessary sand control measures lead to expensive completions and high skins, resulting in low productivity index. On the contrary, inadequate sand control measures may lead to sand production problems, damage to downhole and surface equipment, and costly workover operations. Hence, an accurate prediction of sand production potential is necessary to develop and implement an optimum completion and production strategy.

Sanding is caused by the imbalance between the local stress state of the wellbore and rock strength, therefore factors that influence these stresses and strength impact sanding potential. Factors that can influence the local wellbore stresses include the formation rock strength, the overburden stress, the horizontal stresses, the tectonic stresses, the pore pressure, the drilling process, temperature, and wellbore orientation and inclination. Factors that can influence the rock strength are the confining pressure and chemical interactions between the drilling fluid and the formation.

Well #A is a gas well of Bangladesh which is producing 25 MMSCFD gas currently at 4100 psi well pressure. The gas production rate of this well has been restricted due to potential risk of producing sand. The goal of this sanding potentiality prediction is to use the formation stresses and rock strength information to predict the sanding potentiality over the production life of Well #A.

The sanding potentiality Well #A has been performed by calculating a Critical Drawdown Pressure (CDP) P_{CD} using following four common rock failure criterions:

1. Mohr-Coulomb Failure Criterion
2. Modified-Lade Failure Criterion
3. Mogi-Coulomb Failure Criterion
4. Drucker-Prager Failure Criterion

During these calculations drilling performance parameters, production history, core sample test results, reservoir pressure, and well deviation information were utilized.

1.1. Objectives

The objectives of this study are:

- To determine the rock strength information i.e. Cohesion, Angle of Internal Friction from triaxial test data of Well #A formation rock samples.
- To determine the critical drawdown pressure of a gas well #A in Bangladesh following the four common rock failure criterions as mentioned above.
- To analyze the results of four rock failure criterions and compare with current production and sanding data of gas well #A.

Chapter 2: Literature Review

In this chapter, the rock mechanics, type of rock failure, common rock failure criterion and methods of data acquisition of formation has been discussed briefly.

2.1. Rock Mechanics

The foundation to understanding the sand production is to understand the nature and behavior of rocks that makes up the formation being evaluated. Important concepts include stresses that act upon a rock, rock strength, and the interactions of the two. The fundamental stress and strength terms and concepts are reviewed below. The types and sources of stresses, and the physical and mechanical properties that contribute to rock strength have been included also.

2.1.1. Stress

Stress is a measure of the force applied to a unit surface area. If the force F acting through the cross-section area A, then the Stress σ at the cross-section is defined as:

$$\sigma = \frac{F}{A} \quad \text{......} \quad 2.1$$

The SI unit for stress is Pa (= Pascal = N/m2). In the petroleum industry, “oilfield” units like psi (pounds per square inch) are still extensively used. Stresses are vectors which have both magnitude and direction. In rock mechanics, the sign convention states that compressive stresses are positive. (Fjaer et.al. 2008. P.2)

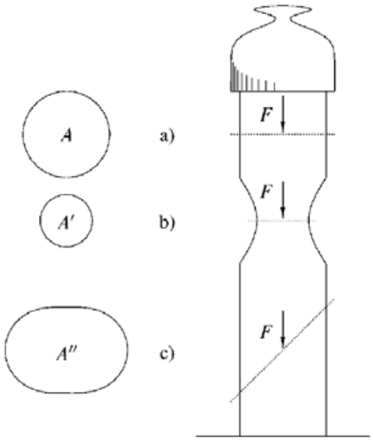

Figure 2-1: Illustration of forces and stress

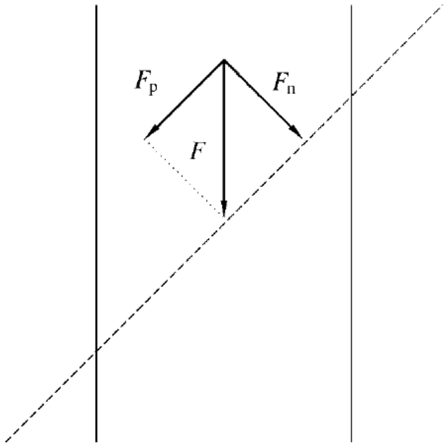

Figure 2-2: Decomposition of forces

As Eq. 2-1 shows, the stress is defined by a force and a cross-section (or more generally, a surface), through which the force is acting. Consider the cross-section at b). The force acting through this cross-section is equal to the force acting through the cross-section at a), (neglecting the weight of the pillar). The area $A^{/}$ of the cross-section at b) is, however, smaller than A. Hence the stress $\sigma = F/A^{/}$ at b) is larger than the stress at a), i.e. the stress depends on the position within the stressed sample.

Consider the cross-section at c) in Fig. 1.1, with area $A^{//}$. Here the force is no longer normal to the cross-section. Decomposing the force into one component F_n that is normal to the cross-section, and one component F_p that is parallel to the section (Fig. 2-2).

The quantity of σ is called Normal Stress.

$$\sigma = \frac{F_n}{A^{"}} \quad \text{...} \quad 2.2$$

While, the quantity of τ is called Shear Stress.

$$\tau = \frac{F_p}{A^{"}} \quad \text{...} \quad 2.3$$

Thus, there are two types of stresses which may act through a surface, and the magnitude of each depends on the orientation of the surface. (Fjaer et.al. 2008. P.3)

2.1.2. Stress Tensor

Stress in three dimensions can be analyzed by studying an infinitesimally small cube. Assuming the material is stationary, the forces on the cube are in equilibrium. Stresses perpendicular to the planes forming the cube are called Normal stresses. Stresses parallel to the planes forming the cube are called Shear stresses. A total of nine stress components related to the cube can exist, three normal stresses and six shear stresses.

The stresses related to a surface normal to the x-axis is denoted as σ_x , τ_{xy} and τ_{xz} representing the normal stress, the shear stress related to a force in y-direction, and the shear stress related to a force in the z-direction, respectively. Physically, there will be only one shear stress associated with this surface. However, the orientation of the shear stress must be identified, and this is most conveniently done by identifying its y- and z-components: τ_{xy} and τ_{xz}. Similarly, the stresses related to a surface normal to the y-axis are denoted $\sigma_{y,}$ τ_{yx} and τ_{yz} while the stresses related to a surface normal to the z-axis are denoted $\sigma_{z,}$ τ_{zx} and τ_{zy}. Thus there are all together nine stress components related to a specific point:

$$\begin{pmatrix} \sigma_x & \tau_{xy} & \tau_{xz} \\ \tau_{yx} & \sigma_y & \tau_{yz} \\ \tau_{zx} & \tau_{zy} & \sigma_z \end{pmatrix} \quad \ldots\ldots\ldots\ldots\ldots\ldots\ldots\ldots\ldots\ldots\ldots\ldots \; 2.4$$

Expression (2.4) is called the stress tensor. It gives a complete description of the stress state at the point P. (Fjaer et.al. 2008. P. 4).

Figure 2-3 shows the relationships of Normal stresses ($\sigma_{x,}$ $\sigma_{y,}$ σ_z) and Shear stresses (τ_{xy}, τ_{yz}, τ_{zx}, τ_{yx}, τ_{zy}, τ_{xz}).

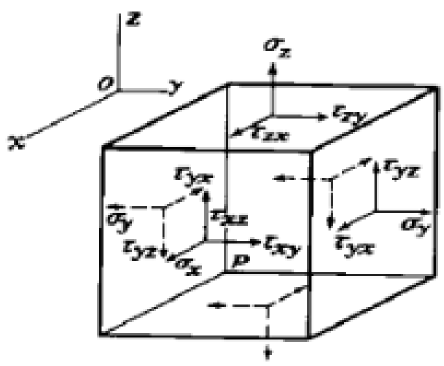

Figure 2-3: Component of Stress

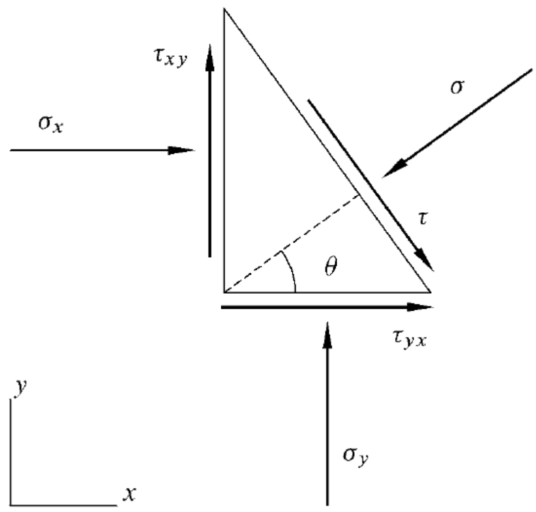

Figure 2-4: Force equilibrium on a triangle.

2.1.3. Principal Stresses in Two Dimensions

The Normal (σ) and Shear (τ) stresses at a surface oriented normal to a general direction θ in the xy-plane, as shown in Fig. 2-4. The triangle on the figure is at rest, such that no net forces act on it. Cancellation of forces implies that:

$$\sigma = \sigma_x cos^2\theta + \sigma_y sin^2\theta + 2\tau_{xy} sin\theta cos\theta \quad \ldots\ldots 2.5$$

$$= \frac{1}{2}(\sigma_x + \sigma_y) + \frac{1}{2}(\sigma_x - \sigma_y)cos2\theta + \tau_{xy} sin2\theta \quad \ldots\ldots 2.6$$

$$\tau = \sigma_y sin\theta cos\theta - \sigma_x cos\theta sin\theta + \tau_{xy} cos\theta cos\theta - \tau_{yx} sin\theta sin\theta \quad \ldots\ldots 2.7$$

$$= \frac{1}{2}(\sigma_y - \sigma_x)sin2\theta + \tau_{xy} cos2\theta \quad \ldots\ldots 2.8$$

By proper choice of θ, it is possible to obtain τ = 0. From Eq. (2.8):

$$tan2\theta = \frac{2\tau_{xy}}{\sigma_x - \sigma_y} \quad \ldots\ldots 2.9$$

The arrows show the direction of the forces on the triangle in Fig-24, assuming that all the stress components are positive.

Eq. (2.9) has two solutions, θ_1 and θ_2. The two solutions correspond to two directions for which the shear stress τ vanishes. These two directions are called the Principal axes of stress. The corresponding normal stresses, σ_1 and σ_2, are called the principal stresses, and are found by introducing Eq. (2.10) into Eq. (2.7):

$$\sigma_1 = \frac{1}{2}(\sigma_x + \sigma_y) + \sqrt{\tau_{xy}^2 + \frac{1}{4}(\sigma_x - \sigma_y)^2} \quad \text{......} \quad 2.10$$

$$\sigma_2 = \frac{1}{2}(\sigma_x + \sigma_y) - \sqrt{\tau_{xy}^2 + \frac{1}{4}(\sigma_x - \sigma_y)^2} \quad \text{......} \quad 2.11$$

A particular coordinate system can be defined where the stress field can be resolved into three normal stresses where no shear stresses exist. These normal stresses are called Principal stresses (σ_1, σ_2 and σ_3). They act perpendicular to the planes along which no shear stresses are present. The Principal stresses are parallel to the axes of the coordinate system. (Fjaer et.al. 2008. P.7)

2.1.4. In-Situ Stress

Prior to drilling, formation rocks are in a balanced or nearly balanced stress state with little or no movement occurring in the rock system. The system is said to be "static" or not in motion. The three principal stresses prior to drilling are called In-Situ stresses. In situ stresses consist of one Vertical stress and two Horizontal stresses, as shown in Figure 2-5.

The in-situ stresses, including overburden and horizontal stresses can be represented in a rectangular coordinate system. The axes of this coordinate system correspond with the direction of the in-situ stresses.

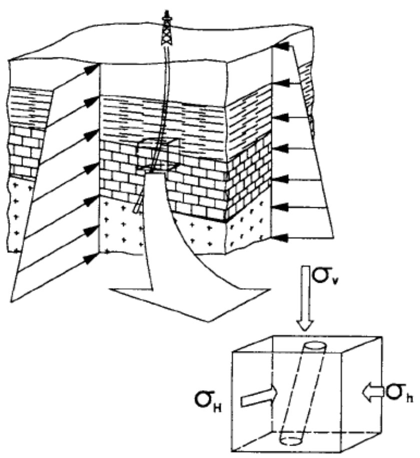

Figure 2-5: In-Situ Stresses

2.1.4.1. Vertical Stress

Vertical stress σ_v(in the pre-drilled formation) is mainly due to gravitational forces. The weight of the overlying formations, with the fluids they contain, is the primary cause of this stress (known as Overburden Stress). (Fjaer et.al. 2008. P. 103)

Overburden or Vertical stress (σ_V) is calculated using Eq. 2-12 where ρ is formation density and h is the thickness of the formation.

$$\sigma_V = \int_0^H \rho(z) g \, dz \quad \text{.......} \quad 2.12$$

When the density log is available, the problem of determining the full in situ stress field is then reduced to determining the magnitude and orientation of the horizontal stresses. However, the density log is rarely available in the first few hundred meters of a well. Then it is necessary to make estimates of the density to obtain the total vertical stress. The average density of sediments in the overburden is between 1.8 and 2.2 g/cm3, so as a rough number, the vertical stress increases downwards with about 20 MPa/km (typically 1 psi/ft). (Fjaer et.al. 2008. P. 103).

2.1.4.2. Horizontal Stress

Horizontal stresses are the two stresses perpendicular to each other in a horizontal plane. Horizontal stress may be due to many sources. One important source of horizontal stress is due to the vertical overburden stress. “As the vertical stress squeezes the rock vertically, it pushes horizontally. Constraint by surrounding rock creates horizontal stress.

The magnitude of horizontal stresses due to overburden can be calculated using inputs of Poisson’s ratio ν, Biot’s constant α, Overburden or Vertical stress σ_V, and the horizontal component of pore pressure. Minimum horizontal stress (σ_h) can be expressed as:

$$\sigma_h = \left(\frac{\nu}{1-\nu}\right) (\sigma_V - Pf) + Pf \quad \text{.......} \quad 2.13$$

When Horizontal stresses are only due to Overburden stress (i.e., a normally stressed area), Horizontal stresses are equal in magnitude (i.e., $\sigma_h = \sigma_H$). Tectonically active areas where faulting or mountains are present or where other geologic anomalies, such as salt domes, exist can add to the horizontal stress and cause unequal horizontal stresses to result. Whenever unequal in situ horizontal stresses exist, these stresses are further distinguished according to their magnitude as either Maximum or Minimum horizontal stresses, σ_H and σ_h respectively.

2.1.5. Wellbore Stresses in Rectangular Coordinate System

The rectangular wellbore coordinate system is a system in which the elemental volume used in examining stresses is rotated until one axis of the coordinate system coincides with the wellbore axis. In-situ stresses are redefined in the rotated coordinate system to aid in defining stresses relative to a planned wellbore. In situ stresses are translated into their normal and shear components to define stresses in the rectangular wellbore coordinate system.

Figure 2-6 illustrates the rectangular wellbore coordinate system in comparison to the In-Situ coordinate system. The stresses associated with each system are shown. In the in situ coordinate system, directions are identified as V (for vertical) and H and h (for the two horizontal directions). The In-Situ stresses associated with these directions are labeled as $\sigma_V, \sigma_h and\ \sigma_H$. In the rectangular wellbore coordinate system, directions are identified as x, y and z, and the associated normal stresses are labeled as $\sigma_x, \sigma_y\ and\ \sigma_{zz}$. σ_{zz} is parallel to the wellbore axis, σ_y and σ_x are in a plane perpendicular to the wellbore axis. (McLean and Addis 1990)

By converting in situ stresses to their vector components, stresses are transformed into the rectangular wellbore coordinate system. The transformed stress state is given as (McLean and Addis 1990)–

$$\sigma_x = \sigma_H sin^2\beta + \sigma_h cos^2\beta \quad \ldots\ldots 2.14$$

$$\sigma_y = cos^2\alpha(\sigma_H cos^2\beta + \sigma_h sin^2\beta) + \sigma_V sin^2\alpha \quad \ldots\ldots 2.15$$

$$\sigma_{zz} = sin^2\alpha(\sigma_H cos^2\beta + \sigma_h sin^2\beta) + \sigma_V cos^2\alpha \quad \ldots\ldots 2.16$$

$$\tau_{xy} = cos\alpha\ sin\beta\ cos\beta(\sigma_H - \sigma_h) \quad \ldots\ldots 2.17$$

$$\tau_{yz} = sin\alpha\ cos\alpha(\sigma_V - \sigma_H cos^2\beta - \sigma_h sin^2\beta) \quad \ldots\ldots 2.18$$

$$\tau_{zx} = sin\alpha\ sin\beta\ cos\beta(\sigma_h - \sigma_H) \quad \ldots\ldots 2.19$$

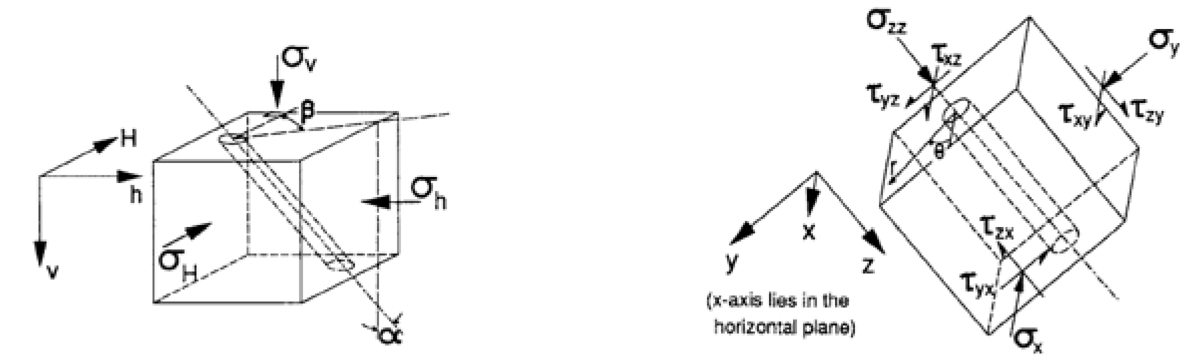

In-Situ Coordinate System

Rectangular Wellbore Coordinate System

Figure 2-6: Defining Stresses in the In-Situ and Rectangular Wellbore Coordinate Systems

2.1.6. Wellbore Stresses in Polar Coordinate System

The use of the polar coordinate system provides a convenient means of defining the near wellbore and wellbore wall stresses. In the polar coordinate system, one axis of the coordinate system is parallel to the axis of the wellbore. Stresses defined in the polar coordinate system are Axial Stress, Radial Stress and Hoop stress. Axial stress is the stress parallel to the wellbore wall. Radial stress is the stress oriented into or away from the center of the wellbore. The tangential stress perpendicular to the radial direction is called hoop stress.

Figure 2-7 shows the stresses along the wellbore wall as defined in a polar coordinate system. Axial stress, oriented into the side of the cube (perpendicular to the page), is not shown in this figure. The angle ϴ is used to locate the elemental volume along the wellbore wall relative to the x-axis in the rectangular wellbore coordinate system. The Axial (σ_z), Radial (σ_r) and Hoop (σ_θ) stresses are translated from the stresses in the x, y, and z direction in the rectangular wellbore coordinate system. (McLean and Addis 1990)

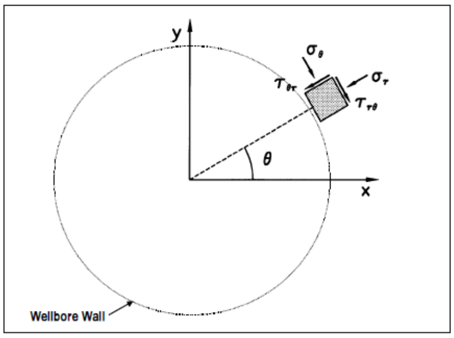

Figure 2-7: Wellbore Stresses in the Polar Coordinate System

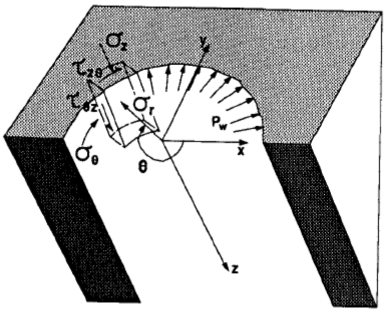

Figure 2-8: Stress State at the Wall of a Deviate Wellbore

Axial, Radial, Hoop, Shear stresses and Pore pressure (the polar coordinate stresses) at the wall of the wellbore can be calculated using the following equations (Ewy et. al. 1990) –

$$\sigma_r = P_w \quad \ldots\ldots 2.20$$

$$\sigma_\theta = \sigma_x + \sigma_y - 2(\sigma_x - \sigma_y)cos2\theta - 4\tau_{xy}sin2\theta - P_w + \alpha_0(P_w - P_F) \quad \ldots\ldots 2.21$$

$$\sigma_z = \sigma_{zz} - \upsilon[2(\sigma_x - \sigma_y)cos2\theta + 4\tau_{xy}sin2\theta] + \alpha_0(P_w - P_F) \quad \ldots\ldots 2.22$$

$$\tau_{\theta z} = 2(\tau_{yz}cos\theta - \tau_{zx}sin\theta) \quad \ldots\ldots 2.23$$

$$P_f = PF + h(Pw - PF) \quad \ldots\ldots 2.24$$

where, $\alpha_0 = k\frac{(1-2\upsilon)}{(1-\nu)}$

P_f is the pore fluid pressure at the wellbore wall.

P_F is the far field formation pressure.

P_w is the well pressure.

k = Biot's Poroelastic Coefficient

ν = Poisson Ratio

h takes on the values 1 and 0 when in underbalance and overbalance respectively. (McLean and Addis 1990). When the well is in production, then there is a communication between the well pressure and the wellbore wall pressure. At this time, the well is underbalance and h = 1 which makes -

$$P_f = Pw \quad \text{.......... 2.25}$$

Most strength criterion are expressed in terms of the Principal Stresses, thus the stresses at the wellbore wall are converted into the three principal stresses (σ_1, σ_2 and σ_3). One of the principal stress acts perpendicular to the wellbore and is simply given by the well pressure, Pw. The remaining two are found by transposing the hoop stress σ_θ, the axial stress σ_z, and the shear stress $\tau_{\theta z}$ (see Figure 2-8), into principal stresses. Thus, the three principal stresses can be expressed as (McLean and Addis 1990) –

$$\sigma_1, \sigma_2, \sigma_3 = \begin{cases} \frac{\sigma_\theta + \sigma_z}{2} + \sqrt{[(\frac{\sigma_\theta - \sigma_z}{2})^2 + \tau_{\theta z}^2]} \\ \frac{\sigma_\theta + \sigma_z}{2} - \sqrt{[(\frac{\sigma_\theta - \sigma_z}{2})^2 + \tau_{\theta z}^2]} \\ P_w \end{cases} \quad \text{.......... } 2.26$$

The ranking shown above implies that Pw = σ_3. This is the most common situation; however, Pw may also be the intermediate or maximum principal stress, depending on conditions. (McLean and Addis 1990)

2.1.7. Effective Stress Concept

Effective stress is the portion of total stress carried by the rock matrix. It is the component of total stress that is most important in evaluating formation stability. Effective stress is expressed as:

$$\sigma' = \sigma - kP_f \quad \text{.......... } 2.27$$

Where, σ' is Effective Stress, σ is the Total Stress, k is Biot's Constant and P_f is the local Pore Pressure. Physically, this means that the solid framework carries the part σ' of the total external stress σ, while the remaining part, kP_f, is carried by the fluid. The remaining pore pressure, $(1 - k)P_f$, is counteracted by internal stresses in the solid. (Fjaer et.al.P.32)

Biot's constant (k) is the effectiveness of pore fluid in supporting the stress, and is a function of matrix solid bulk modulus (Ks) and bulk modulus of the drained frame (K_{fr}) of the rock is expressed as:

$$k = 1 - \frac{K_{fr}}{K_s} \quad \text{.......... } 2.28$$

Where, K_{fr} is the bulk modulus of the framework or frame modulus and K_s is the bulk modulus of the solid grains.

The effective stress concept as given by Eq. 2-27 in terms of the Biot's constant α, was derived under the assumption that the rock is linearly elastic, and is not directly applicable for a rock at failure. It is, however, generally accepted that Terzaghi's definition of effective stress (Fjaer et.al. 2008 P76)-

$$\sigma' = \sigma - P_f \quad \text{.......} \quad 2.29$$

And appears to be the most relevant definition to be used in failure criteria. Inserting Eq. 2-25 in Eq. 2-29 the effective stress equation can be presented as:

$$\sigma' = \sigma - P_w \quad \text{.......} \quad 2.30$$

So the effective principal stresses can be expressed as –

$$\sigma_1' = \sigma_1 - P_w \quad \text{.......} \quad 2.31$$

$$\sigma_2' = \sigma_2 - P_w \quad \text{.......} \quad 2.32$$

$$\sigma_3' = \sigma_3 - P_w \quad \text{.......} \quad 2.33$$

2.1.8. Critical Drawdown Pressure

Critical Drawdown Pressure, P_{CD} is the maximum difference between reservoir pressure P_F and minimum well bottom hole flowing pressure P_w that the formation can withstand without sand being produced along with the formation fluid. In this exercise, a negative critical drawdown pressure indicates that the formation will produce sand during the production of formation fluids.

$$P_{CD} = P_f - P_{W,Min} \quad \text{.......} \quad 2.34$$

2.2. Type of Formation Rock Failure

When rock material is removed from the wellbore, the rock material at and near the wellbore wall must support in situ stresses as well as the stresses that were previously supported by the removed material. Stresses greater than those of the surrounding in situ stresses result disturbance at the wellbore wall. Also during the production time, if the wellbore pressure drops below wellbore minimum pressure $P_{W,Min}$ the formation can also be damaged which can result sand production. In this chapter the common formation failure modes (tensile, compressional or shear) have been discussed, so that precautions can be made to prevent it from happening.

2.2.1. Tensile Failure

Tensile failure occurs when the effective tensile stress across some plane in the sample exceeds the tensile strength of the rock which is denoted as T_0, and has the same unit as stress. The tensile strength is a characteristic property of the rock.

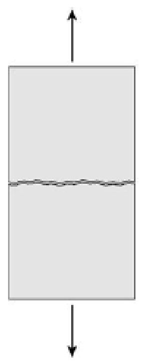

Figure 2-9: Tensile Failure

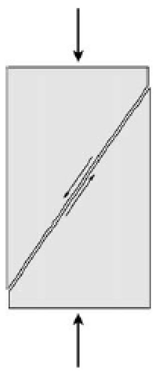

Figure 2-10: Shear Failure

The failure criterion, which specifies the stress condition for which tensile failure will occur is given as (Fjaer et.al. 2008. P. 59):

$$\sigma' = -T_0 \quad \text{......} \quad 2.35$$

For isotropic rocks, the conditions for tensile failure will always be fulfilled first for the lowest principal stress, so that the tensile failure criterion becomes (Fjaer et.al. 2008. P. 59) -

$$\sigma_3' = -T_0 \quad \text{......} \quad 2.36$$

2.2.2. Shear Failure

Shear failure occurs when the shear stress along some plane in the sample is sufficiently high. Eventually, a fault zone will develop along the failure plane, and the two sides of the plane will move relative to each other in a frictional process, as shown in Fig. 2-10. (Fjaer et.al. 2008 P.60)

It is well known that the frictional force that acts against the relative movement of two bodies in contact depends on the force that presses the bodies together. It is therefore reasonable to assume that the critical shear stress (τ_{max}) for which shear failure occurs, depends on the normal stress (σ') acting over the failure plane. That is:

$$|\tau_{max}| = f(\sigma') \quad \ldots\ldots\ldots\ldots\ldots\ldots\ldots\ldots\ldots\ldots\ldots\ldots\ldots \; 2.37$$

This assumption is called Mohr's hypothesis. (Fjaer et.al. 2008 P.60)

2.2.3. Compaction Failure

Pore collapse is a failure mode that is normally observed only in high porosity materials, where the grain skeleton forms a relatively open structure. When the material is compressed, grains may loosen or break and then be pushed or twisted into the open pore space, resulting in a closer packing of the material. The process is called compaction. This deformation mode is schematically illustrated in Fig. 2-11. (Fjaer et.al. 2008. P. 67)

Pore collapse may occur under pure hydrostatic loading. Microscopically, however, failure will be due to local excessive shear forces acting through grains and grain contacts. From this point of view, pore collapse may be regarded as distributed shear failure within the material. (Fjaer et.al. 2008. P. 67).

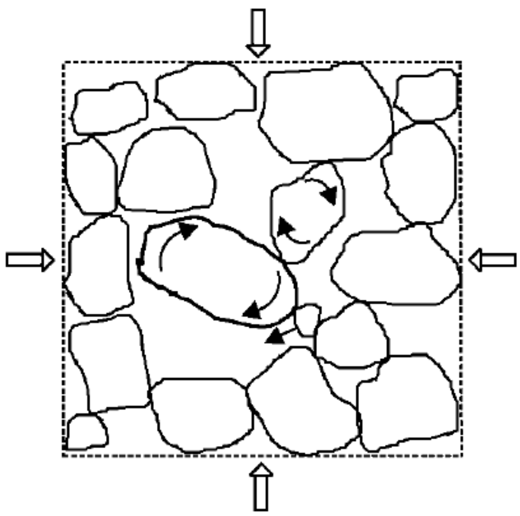

Figure 2-11: Grain reorientation resulting in a closer packing

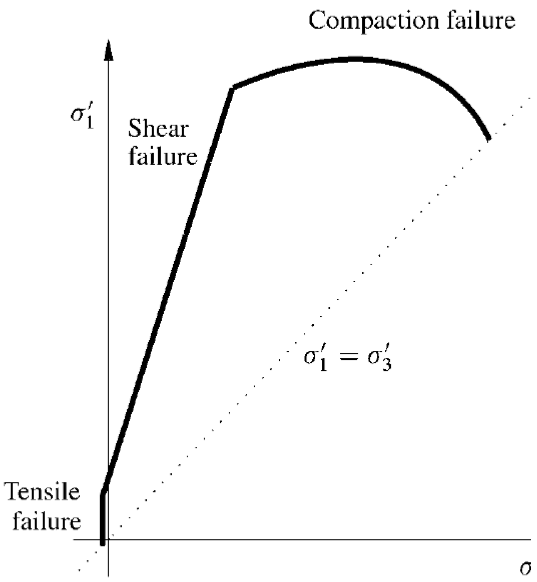

Figure 2-12: Location of the various failure modes in principal stress space

2.3. Formation Rock Failure Criterion

In order to evaluate the wellbore stability and sanding potential, a realistic constitutive model must be used to compute the stresses around the wellbore. The computed stresses must then be compared against a given failure criterion. Numerous failure criterions are available to explain the formation rock failure. Here the four most important and common criterions have been discussed.

2.3.1. Mohr-Coulomb failure criterion

In the τ-σ' plane, Eq. 2-37 describes a line that separates a "safe region" from a "failure" region. The line is sometimes referred to as the failure line or the failure envelope in the Mohr-Coulomb Criterion. An example is shown in Fig. 2-13, where three principal stresses and the Mohr's circles connecting them have been indicated. For a given set of principal stresses all possible combinations of τ and σ' lie within the area in between the three circles (i.e. the shaded area of Fig. 2-13). (Fjaer et.al. 2008. P 60)

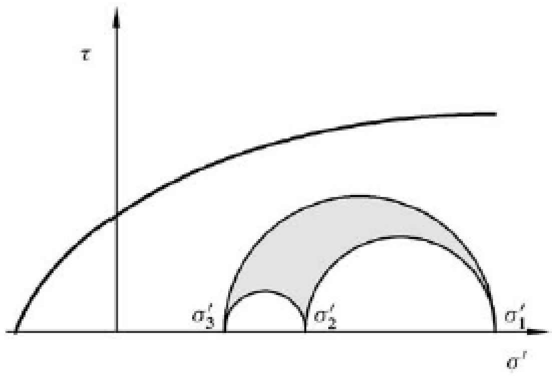

Figure 2-13: Failure line in the Shera Stress-Normal Stress Diagram

The stress state of Fig. 2-13 represents a safe situation, as no plane within the rock has a combination of τ and σ' that lies above the failure line. But if σ_1' is increased then the circle connecting σ_1' and σ_3' will expand, and eventually touch the failure line. The failure criterion is then fulfilled for some plane(s) in the sample, and the sample fails. Here the value of the intermediate principal stress (σ_2') has no influence on this situation. Since σ_2' by definition lies within the range (σ_3', σ_1'), it does not affect the outermost of Mohr's circles and hence it does not affect the failure. Thus, pure shear failure, as defined by Mohr's hypothesis, depends only on the minimum and maximum principal stresses and not on the intermediate stress. (Fjaer et.al. 2008. P 60)

This criterion relates the shearing resistance to the contact forces and friction, to the physical bonds that exist among the rock grains. The Mohr-Coulomb criterion is based on the assumption that f($\boldsymbol{\sigma'}$) is a linear function of $\boldsymbol{\sigma'}$(Fjaer et.al. 2008 P. 61):

$$|\tau| = s_0 + \sigma' tan\varphi \quad \text{..} \quad 2.38$$

Where, τ = Shear Stress, S_0 = Cohesive Strength, ϕ = Angle of internal Friction and σ = Effective Normal Stress acting on the grain. (Fjaer et.al. 2008. P 61)

In Fig. 2-14, the MC failure envelop is determined by several Mohr's circles where each circle is one Triaxial test. (Immerstein 2013 P. 37). The failure envelop is the best fit straight-line tangent with all Mohr circle. The intersection of straight line Mohr Envelop with y axis provides the Cohesion S_0 value and the angle with x axis provides the Angle of Internal Friction ϕ.

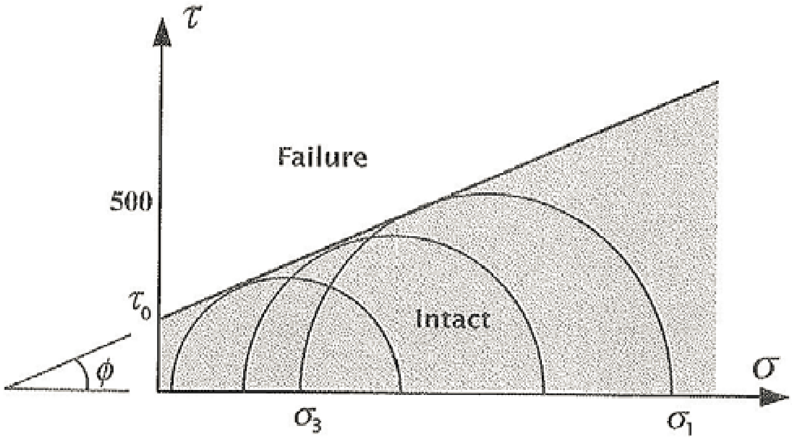

Figure 2-14: Mohr-Coulomb failure model from Triaxial test data

However, the Cohesion S_0 and Angle of Internal Friction ϕ can be also derived from ultimate Axial Stress-Confining pressure Curve. In this curve, the Axial Stress and Confining stress data from multiple Triaxial test are plotted in y and x axis respectively. The straight line trend of the data points intersects with y axis provides the Unconfined Compressive Strength C_0. The slop of the trend provides the Angle of Internal Friction ϕ value.

According to Coulomb failure Criterion, the Unconfined Compressive Strength C_0 and Angle of Internal Friction ϕ are determined from the ultimate Axial Stress-Confining pressure curve (Fig 2-15) which is developed from the Triaxial test data.

$$\phi = sin^{-1}\left(\frac{m-1}{m+1}\right) \quad \text{.......... } 2.39$$

$$C_0 = 2S_0\frac{cos\phi}{1-sin\phi} \quad \text{..........} 2.40$$

$$S_0 = \frac{C_0(1-sin\phi)}{2cos\phi} \quad \text{..........} 2.41$$

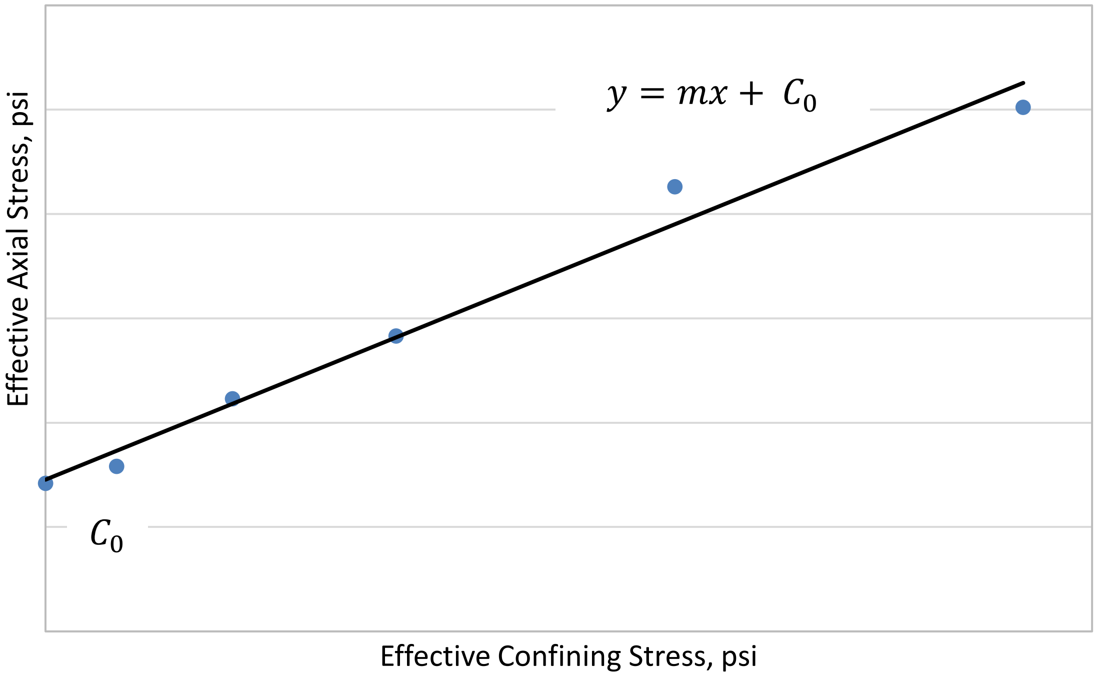

Figure 2-15: Ultimate Axial Stress-Confining Pressure Curve

In Fig. 2-16, Mohr–Coulomb criterion has been drawn and the Mohr's circle touches the failure line.

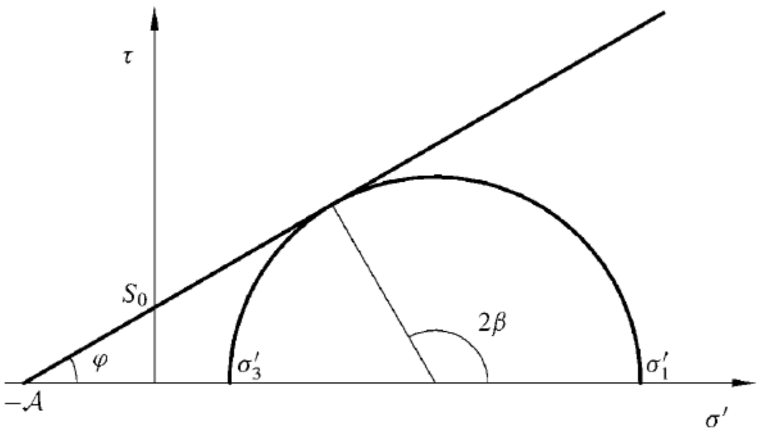

Figure 2-16: Mohr–Coulomb criterion in τ–σ' space with Mohr's circle corresponding to a critical stress state.

Mohr-Coulomb failure criterion Eq. 2-37 can be expressed by Principal stresses and Effective Principal Stresses (Fjaer et.al. 2008 P63):

$$\sigma_1' = 2S_0 \frac{cos\phi}{1-sin\phi} + \sigma_3' \frac{1+ sin\phi}{1-sin\phi} \quad \text{……} \; 2.42$$

$$(\sigma_1 - P_f) = 2S_0 \frac{cos\phi}{1-sin\phi} + \left(\sigma_3 - P_f\right) \frac{1+ sin\phi}{1-sin\phi} \quad \text{……} \; 2.43$$

From Eq. 2-25, the Mohr-Coulomb failure criterion can be expressed as -

$$(\sigma_1 - P_w) = 2S_0 \frac{cos\phi}{1-sin\phi} + (\sigma_3 - P_w) \frac{1+sin\,\phi}{1-sin\phi} \quad \text{……} \; 2.44$$

The Mohr Coulomb Failure Criterion will be,

$$F = 2S_0 \frac{cos\phi}{1-sin\phi} + (\sigma_3 - P_w) \frac{1+ sin\phi}{1-sin\phi} - (\sigma_1 - P_w) \quad \text{……} \; 2.45$$

$$or, \quad F = 2S_0 \frac{cos\phi}{1-sin\phi} + \sigma_3' \frac{1+sin\,\phi}{1-sin\phi} - \sigma_1' \quad \text{……} \; 2.46$$

The rock Shear failure will start occurring if F equals to zero or negative (F ≤ 0).

2.3.2. Drucker-Prager failure criterion

The Drucker-Prager Criterion can be expressed in terms of effective principal stresses as follows (Zhang et. al. 2010 and Alejano and Bobet. 2012):

$$\sqrt{J_2} = \alpha I_1 + k \quad \text{……} \; 2.47$$

Where, $I_1$and J_2 are respectively the First Stress Invariant and the Second Deviatoric Stress Invariant defined by (Zhang et. al. 2010 and Alejano 2012),

$$I_1 = \sigma_1' + \sigma_2' + \sigma_3' \quad \text{……} \; 2.48$$

$$J_2 = \frac{(\sigma_1' - \sigma_2')^2 + (\sigma_2' - \sigma_3')^2 + (\sigma_3' - \sigma_1')^2}{6} \quad \text{……} \; 2.49$$

and α and k are material constants which can be determined by matching two particular points with those of the Mohr-Coulomb criterion.

The material constants in the Drucker–Prager criterion can be related to the Mohr–coulomb parameters in several ways by matching these two criteria. For example, if the matching points are selected in such way that the Drucker–Prager failure surface circumscribes the Mohr–Coulomb hexagonal pyramid, α and k can be related to

Cohesion S_0 and Angle of Internal Friction φ as follows (Zhang et. al. 2010 and Alejano 2012):

$$\alpha = \frac{2sin\phi}{\sqrt{3}(3-sin\phi)} \quad \text{........ 2.50}$$

$$k = \frac{6\ S_0 cos\phi}{\sqrt{3}(3-sin\phi)} \quad \text{........ 2.51}$$

It can be seen that the intermediate principal stress σ_2' has a great influence on rock strength, according to the Drucker-Prager Criterion.

The Drucker-Prager Failure Criterion can be expressed as,

$$F = \alpha I_1 + k - \sqrt{J_2} \quad \text{........ 2.52}$$

The rock Shear failure will start occurring if F equals to zero or negative (F ≤ 0).

2.3.3. Mogi-Coulomb failure criterion

Al-Ajmi and Zimmerman was first out to introduce the Mogi-Coulomb failure criterion in 2006. They found some weaknesses in the criterions that already existed. When they were analyzing their failure data they saw that the Drucker-Prager criterion overestimated rock strength, while the Mohr-Coulomb criterion underestimated it. They argued that the intermediate principle stress has an effect on the failure of the rock, and that the so called Mogi-Coulomb criterion would give the best fit. The criterion can be written much like the Mohr-Coulomb, as (Zhang et. al. 2010, Al-Ajmi and Zimmerman 2006):

$$\tau_{oct} = a + b\sigma_{m,2}' \quad \text{........ 2.53}$$

Where $\sigma_{m,2}'$ and τ_{oct} are respectively the effective mean stress and the octahedral shear stress defined by,

$$\sigma_{m,2}' = \frac{\sigma_1' + \sigma_3'}{2} \quad \text{........ 2.54}$$

$$\tau_{oct} = \frac{1}{3}\sqrt{(\sigma_1' - \sigma_2')^2 + (\sigma_2' - \sigma_3')^2 + (\sigma_3' - \sigma_1')^2} \quad \text{........ 2.55}$$

And a and b are material constants which are simply related to cohesion S_0 and angle of friction φ as follows (Zhang et. al. 2010, Al-Ajmi and Zimmerman 2006):

$$a = \frac{2\sqrt{2}}{3} S_0 cos\phi \quad \text{.......... 2.56}$$

$$b = \frac{2\sqrt{2}}{3} \ sin\phi \quad \text{.......... 2.57}$$

It can be seen that the Mogi-Coulomb criterion, as the modified Lade criterion predicts a strengthening effect of the intermediate principal stress σ_2' followed by a reduction in strength once σ_2' becomes too high.

Mogi-Coulomb Failure Criterion can be expressed as:

$$F = a + b\sigma_{m,2}' - \tau_{oct} \quad \text{.......... 2.58}$$

The rock Shear failure will start occurring if F equals to zero or negative (F ≤ 0).

2.3.4. Ewy Modified Lade Failure criterion

Several researchers have proposed three-dimensional rock failure criteria that predict the effect of the intermediate principal stress much more accurately than either the Mohr–Coulomb or the Drucker–Prager criteria. Modified Lade criterion has the following desirable qualities:

1. It correctly describes the influence of the intermediate principal stress on rock strength, and therefore on wellbore stability.
2. It can be rearranged to give a closed-form solution for critical mud weight, for any wellbore orientation
3. Only two rock strength parameters are required, such as cohesion and friction angle. (Ewy R. T. 1999 and Zhang et.al. 2010).

Defining appropriate stress invariants I_1'' and I_3'' Modified Lade Failure criterion can be presented as (Ewy et.al. 1999 and Zhang et. al. 2010):

$$\frac{(I_1'')^3}{I_3''} = 27 + \eta \quad \text{.......... 2.59}$$

Where,

$$I_1^{''} = (\sigma_1 + S_1 - p_f) + (\sigma_2 + S_1 - p_f) + (\sigma_3 + S_1 - p_f) \quad \text{.........................} \quad 2.60$$

$$I_3^{''} = (\sigma_1 + S_1 - p_f)(\sigma_2 + S_1 - p_f)(\sigma_3 + S_1 - p_f) \quad \text{.....................................} \quad 2.61$$

S_1 and η are material constants and p_f is the wellbore pore pressure. The parameter C_0 is the Unconfined Compressive Strength of the rock, while the parameter η represents the internal friction. Calculations show that these parameters can be directly derived from the Mohr– Coulomb cohesion S_0 and friction angle ϕ by:

$$C_0 = \frac{S_0}{tan\phi} \quad \text{...} \quad 2.62$$

$$\eta = \frac{4\, tan^2\phi\ (9-7\ sin\phi)}{(1-sin\phi)} \quad \text{...} \quad 2.63$$

Where, S_0 and ϕ are determine from Triaxial compression tests (Ewy et. al. 1999).

Rearranging Eq. 2-59 in to a Failure Function F, given by (Ewy et. al. 1990)

$$F = (27 + \eta) - \frac{(I_1^{''})^3}{I_3^{''}} \text{...} \quad 2.64$$

When the value of the function F is positive, the wellbore is stable, and when F is negative, the wellbore is unstable. (McLean and Addis 1990)

2.4. Formation Mechanical Properties and Stress Data Acquisition

In this chapter, some popular testing methods have been discussed to estimate mechanical properties of formation rock and in-situ stresses. All these testing and data acquisition methods can be grouped in to three categories which are as follows:

- Laboratory Core Test

- Measurement while drilling

- Wireline Logging methods

2.4.1. Laboratory Core Tests

Laboratory measurement of rock strength can be physically achieved through testing of a core sample extracted from the formation. Uniaxial Core Test, Tri-axial Core Test and Hole Collapse Test are common core tests performed in the laboratory. Fig. 2-17 illustrates the stress to core relationships for each type of core test.

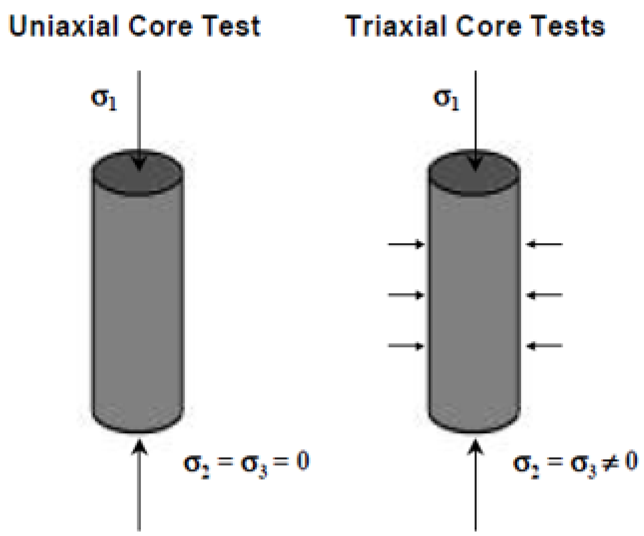

Figure 2-17: Illustration of Core Testing

2.4.1.1. Uniaxial Core Test

The Uniaxial Core Test is an unconfined test in which a force is applied parallel to the axis of the core sample. No lateral forces are applied and therefore the sample is unconfined. The magnitude of applied stress is increased until sample failure is reached. The stress at failure is the Unconfined Compressive Strength (UCS), which is a measure of a rock’s strength expressed as the amount of stress a rock can withstand (when unconfined laterally) without failing. This test also provides data for Young’s modulus and Poisson’s ratio.

2.4.1.2. Tri-axial Core Test

The Tri-axial Core Test is a confined test that measures strength at different levels of confining pressure. Axial σ_z and confining pressure σ_r are applied to the sample, increasing simultaneously until the test pressure reaches to reservoir Pore Pressure P_f. The confining pressure σ_r is then held constant while the axial pressure σ_z is increased until failure of the sample occurs. This test yields confined compressive strength (CCS). Multiple confined core tests are used to determine Cohesion S_O and Angle of Internal Friction ϕ. It is also used to measure elastoplastic stress-strain behavior. Fig. 2-18 shows the test apparatus for the Tri-axial core test.

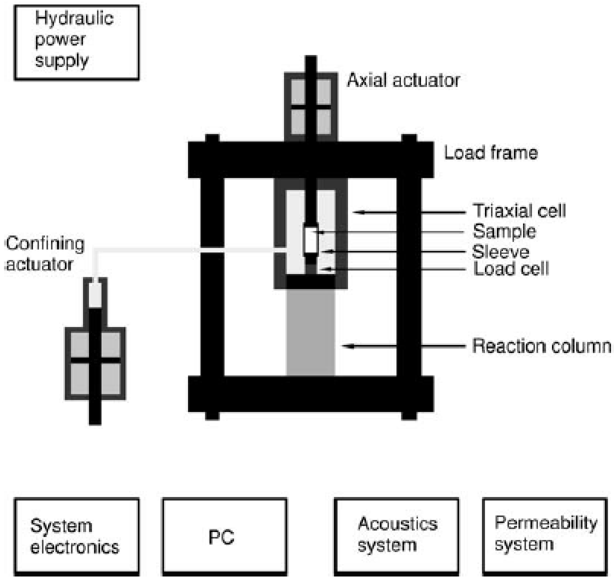

Figure 2-18: Schematic drawing of Tri-axial Test Cell (Fjaer et.al. 2008. P. 265)

By performing a series of tests at different confining pressures, it is possible to map the entire failure envelope. Care should be taken that sufficient data is collected at low confining pressures, representing the stress state near the borehole. The maximum confining pressure should correspond to the minimum principal effective stress far from the borehole. For a producing reservoir, the value at maximum depletion should be selected (Fjaer et.al. 2008. P. 265)

2.4.1.3. Hole Collapse Test

The Hole Collapse Test is a laboratory testing procedure using the Tri-axial cell and a hollow rock sample to simulate wellbore situations. In a hole collapse test, a hollow cylinder of formation material is externally stressed until collapse occurs. The desirable features of such a test are1) the geometry simulates the loading of a wellbore or perforation under downhole conditions and 2) the stabilizing effects of non-linear and/or plastic rock deformations are included in the measurement of collapse pressure. The test provides a direct measure of the stress required to cause hole failure in the formation of interest. (Ewy et. al. 1990)

Hole collapse specimen after sample failure

Figure 2-19: Sample of Hole Collapse Test (Ewy et. al. 1990)

2.4.2. Measurement While Drilling

Common field tests during drilling are the FIT (Formation Integrity Test) and LOT (Leak-Off Test). When drilling a well it is common practice to perform a Pressure Integrity Test (PIT) after each hole section has been drilled to test that the cement job is good enough for further drilling.

2.4.2.1. Formation Integrity Test (FIT)

Formation Integrity Test is often used instead of a LOT or a XLOT. While drilling a well, FIT is performed when while pumping up the pressure in the well but is stopped before reaching the leak-off pressure. The trend of the test will therefore show a near linear trend when plotted as pressure against volume pumped. A disadvantage when using FIT is that it will not give any information about the principle stresses in the formation around the wellbore. The test will only verify that the casing shoe can withstand the pressure that is required to drill the next section according to the drilling program. One advantage of using the FIT is that it do not create a fracture in the formation, and the integrity of the well will therefore be intact. (Immerstein 2013 P. 53)

2.4.2.2. Leak-off Test (LOT)

Leak-off tests (LOT) are performed during the drilling phase of a well, in the formation immediately below each casing shoe. The purpose of this test is to determine the maximum well pressure the new borehole section can sustain without fracturing and loss of drilling fluid. A traditional leak-off test is therefore not designed to determine the smallest horizontal stress, but to obtain a design value for the mud density in the next borehole section which is going to be drilled.

After a casing string has been cemented, the casing shoe is drilled out and a few meters of new formation is penetrated. A leak-off test is then performed by pressurizing this open-hole section. The principle of a leak-off test is shown in the first cycle in Fig. 2-12. The pressure in the hole is increased by pumping at a constant volume rate, typically 50–250 l/min. This yields a straight line of pressure versus volume (time), with the slope of the line given by the compressibility of the system (primarily the drilling fluid). The point where the pressure response starts to deviate from this straight line is defined as the leak-off point. This is actually the point where a fracture is starting to initiate. Normally, a leak-off test is stopped shortly after this, even if the pressure continues to increase above the leak-off pressure. (Fjaer et.al. 2008. P. 300)

2.4.2.3. Extended Leak-off Tests

The leak-off point or fracture initiation point is, however, not necessarily directly related to the smallest horizontal stress, and is therefore no estimate of σ_h. It is also important to note that if the test is stopped shortly after the leak-off point, the generated fracture is very short, and even if the shut-in phase is recorded (Fig. 2-20), this shut-in pressure may significantly overestimate the smallest horizontal stress. Thus using the leak-off pressure as an estimate of the smallest horizontal stress can cause significant errors. At the very best, the smallest horizontal stress will be a lower bound to a large population of leak-off pressures (Fjaer et.al. 2008. P. 300)

To make the leak-off test applicable for stress determination, modifications have to be made. This has led to the so-called extended leak-off test (XLOT, ELOT). The main difference from the standard leak-off test is that pumping continues well beyond the leak-off point and also beyond the breakdown pressure. To get a reliable stress estimate, pumping should continue until stable fracture growth is obtained. After shut-in, the shut-in/decline phase should be recorded. As illustrated by Fig. 2-20, it is recommended to pump several cycles to obtain repeatable test results. (Fjaer et.al. 2008. P. 301)

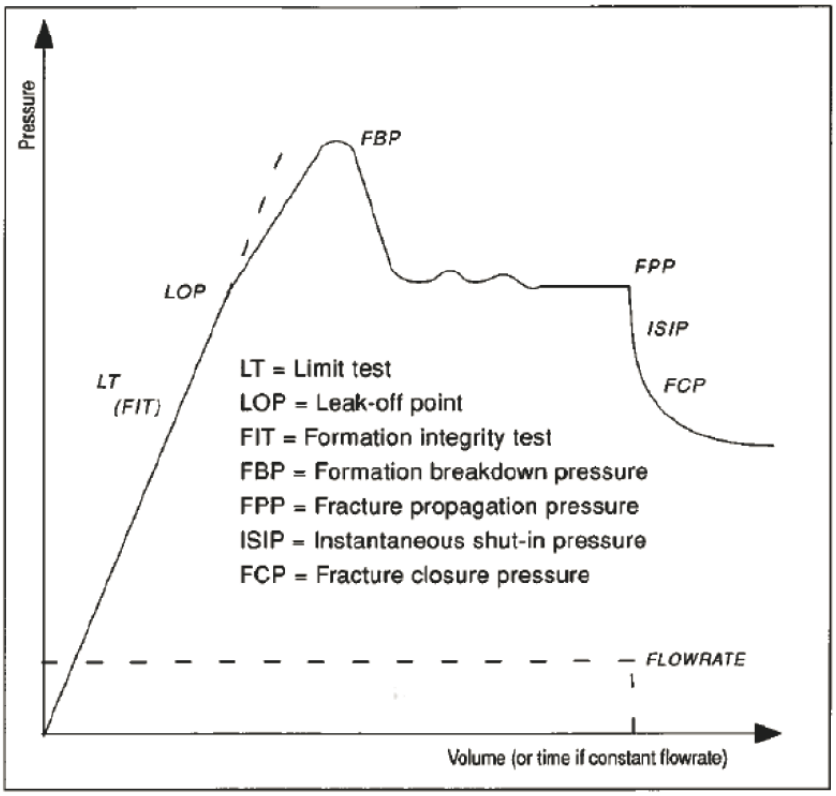

Figure 2-20: Extended Leak-Off Test showing pressure as a function of volume

2.4.2.4. Drilling Data

The response of the drill bit should reflect the mechanical properties of the rock, under true downhole conditions. Bit response is, however, also dependent on a number of other parameters. Traditionally, the motivation for rock-bit interaction models has been to improve bit selection and bit operation procedures. The process of cuttings generation and cuttings removal is fairly complicated, and most ROP (rate of penetration) models are therefore empirical or semi-empirical. Although ROP models are available for several bit types, most of the modelling efforts have been directed towards roller cone bits. A representative version of an ROP model is (Fjaer et.al. 2008. P. 295):

$$R = \left(\frac{aS^2D^3}{nW^2} + \frac{b}{ND} + \frac{cD\rho\mu}{F_m}\right)^{-1} \quad \text{.........} \quad 2.65$$

Where, R = Rate of Penetration, W = Weight on bit, N = Bit Rotary Speed, S = Rock Strength, D = Bit Diameter, F_m = Modified Jet Impact Force, ρ = Mud Density, μ = Plastic Viscosity and a, b, c = Dimensionless constants.

Additional effects related to bit wear and chip hold down may also be included. Thus one can also solve the equation for rock strength when the rate of penetration and the other parameters and function are known. (Fjaer et.al. 2008. P. 295).

2.4.3. Wireline Logging Methods

The most important method for estimation of elastic parameters is acoustic logging, and in particular acoustic wireline logs. Acoustic logging while drilling is now also available, but is still less used.

2.4.3.1. Acoustic wireline logging

The primary output from acoustic logging tools is the velocities and waveforms of different waves, such as the compressional (P), shear (S) and Stoneley waves. Note that acoustic logging tools may be used to generate information about a number of other characteristics of the formation, such as lithology identification, porosity estimates, gas detection, detection of natural fractures, and qualitative evaluation of permeability variations and creation of synthetic seismograms for comparison with surface seismic (Fjaer et.al. 2008. P.290)

From a mechanical properties point of view, one is most interested in the shear velocity in slow formations, since low wave velocities indicate low strength and hence potential stability and sanding problems. Direct measurement of both compressional and shear velocities also in slow formations is possible using dipole or multipole tools. From the Compressional and Shear Wave velocity information, dynamic Young's Modulus (E_{dyn}) and dynamic Poisson's Ratio (ν_{dyn}) are calculated using the following equations: (Fjaer et.al. 2008. P. 289)

$$E_{dyn} = \frac{\rho v_s^2 (3v_p^2 - 4v_s^2)}{(v_p^2 - v_s^2)} \quad \text{..................} \quad 2.66$$

$$\nu_{dyn} = \frac{v_p^2 - 2v_s^2}{2(v_p^2 - v_s^2)} \quad \text{..................} \quad 2.67$$

Where,

ρ = Density

v_s = Shear Wave S-Wave Velocity

v_p = Primary Wave or P-Wave velocity

2.4.3.2. Acoustic Logging while drilling

In recent years, tools for acoustic logging while drilling have also become available. The tool configuration is similar to that shown in Fig. 2-21, with a transmitter separated a few feet (typically 4–7 ft) from an array of receivers. The full waveforms are normally recorded in a downhole memory for later evaluation, but transit times can be transmitted up hole for real time use: lithology evaluation, porosity determination, pore pressure estimation and correlation of drill bit position to seismic maps.

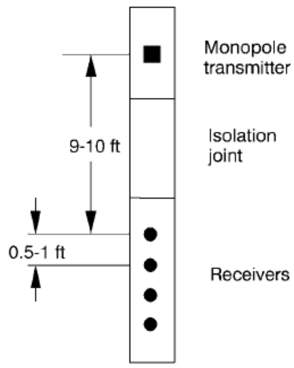

Figure 2-21: Principal Sketch of a full waveform sonic tool

Real time access to good estimates of mechanical properties of the rock is obviously useful also for borehole stability evaluation while drilling. By logging while and after drilling one could possibly monitor changes in the rock response during the open-hole period. This may give an early warning of possible deterioration of rock integrity with time which eventually results in borehole stability problems (Fjaer et.al. 2008 P.292).

2.4.3.3. Density Log (Overburden Stress)

The density log is useful for determining mechanical properties in two manners: first, the density is needed to convert from acoustic velocities to dynamic elastic moduli.

Second, the density integrated over the vertical depth of the well is usually considered to give a good estimate of the vertical stress, at least in areas of low tectonic activity. In such areas, the vertical stress is also considered to be a principal stress. When the density log is available, the problem of determining the full in situ stress field is then reduced to determining the magnitude and orientation of the horizontal stresses [Fjaer et.al. 2008 P.296]. As discussed earlier, Overburden or Vertical stress (σ_V) is calculated using the below equation where r is formation density and h is the thickness of the formation.

$$\sigma_V = \int_0^H \rho(z) g \, dz \quad \text{......} \quad 2.68$$

However, the density log is rarely available in the first few hundred meters of a well. Then it is necessary to make estimates of the density to obtain the total vertical stress. It is common to assume a density in the range 1.8–2.0 g/cm^3 (Fjaer et.al. 2008 P.296) and as a rough number, the vertical stress increases downwards with about 20 MPa/km (typically 1 psi/ft) (Fjaer et.al. 2008 P.103).

2.4.3.4. Borehole logs (Horizontal Stress Directions)

Determination of horizontal stress directions is based on the possibility of failure at the borehole wall which can be detected by borehole logging tools. To be detectable, the failures must occur in the period after drilling and prior to logging. In a vertical borehole which penetrates layers of significantly different horizontal stresses ($\sigma_H > \sigma_h$), two distinct failure modes can be detected: compressive and tensile failure. The directions of these two failure modes in an idealized situation are uniquely given by the directions of the two principal horizontal stresses, as illustrated in Fig. 2-22. Compressive failure or shear failure will be induced in the direction parallel with the smallest horizontal stress (σ_h) if the well pressure is low enough to induce shear failure. This is commonly referred to as breakouts in this context and will lead to an ovalization of the borehole. Tensile failure will occur in the direction parallel with the largest horizontal stress (σ_H) if the well pressure is large enough to induce fracturing.

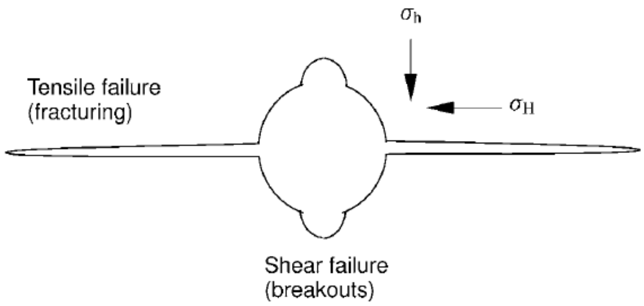

Figure 2-22: Illustration of directions for compressive and tensile failure around a vertical borehole.

In the Figure 2-22, since tensile failure occurs at high well pressures and compressive failure at low pressures, these failure modes are not normally observed at the same depth. A possible exception is if there has been a large variation in the well pressure.

Once a failure has occurred on the borehole wall, it is tempting to try to back-calculate also stress magnitudes, especially the magnitude of the largest horizontal stress by using elastic theory and appropriate failure criteria. However, a number of assumptions are required for such analyses, rendering the results uncertain (Fjaer et.al. 2008. P. 297).

2.4.3.5. Caliper logs

The caliper log (four-arm) has commonly been used to estimate horizontal stress directions from breakout orientations. This tool provides two diameters of the borehole cross-section. To be able to identify stress induced borehole breakouts, a set of identification criteria has to be implemented (Fjaer et.al. 2008. P. 297)

- The tool is rotating above and below a borehole breakout.
- The rotation stops over the breakout zone.
- The borehole elongation is clearly seen in the log. One pair of pads must show a relatively sharp ascent and descent of the borehole diameter.
- The smaller of the caliper readings is close to bit size, or if the smaller caliper reading is greater than bit size it should exhibit less variation than the larger caliper.
- The direction of elongation should not consistently coincide with the high side of the borehole when the hole deviates from vertical.

2.4.3.6. Image Logs

Image logs include both electrical (resistivity) and acoustical borehole imaging logs. The electrical image log operates with a large number of electrodes in contact with the formation, usually distributed over several pads on independent arms (four or six). This shallow electrical investigation is well suited for investigation of fine structures like bedding planes, natural fractures and also drilling induced fractures.

The acoustical imaging tool (often referred to as borehole televiewer, BHTV) is based on reflection of acoustic waves from the borehole wall, recording the travel time and amplitude of the reflected pulses. The pulses are generated by a rapidly rotating piezo-electric crystal, thus creating a helix-shape logging path with a short distance between each revolution. This tool is best suited for detection of borehole breakouts, as drilling induced fractures do not create significant changes in borehole radius or reflectivity. Since these tools provide a full image of the borehole wall, it is possible to distinguish between stress induced breakouts and keyseats. An example of an electrical borehole image log has been shown in Fig. 2-23. (Fjaer et.al. 2008. P. 298).

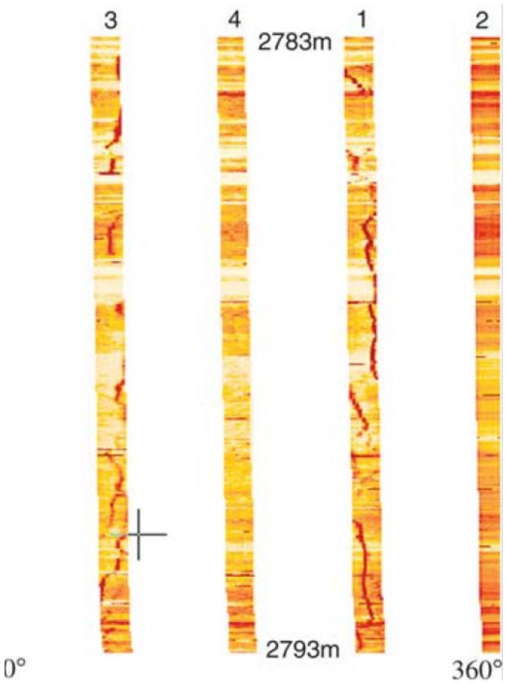

Figure 2-23: A resistivity Image Log of a North Sea Well (Fjaer et.al. 2008. P. 299).

Chapter 3: Outlined Methodology

In this work, the potential of sanding from a producing wellbore has been studied by applying four most common rock failure criterions to calculate the Critical Drawdown Pressure $P_{CD.}$ These criterions are:

1. Mohr-Coulomb Failure Criterion
2. Modified Lade Failure Criterion
3. Mogi-Coulomb Failure Criterion
4. Drucker-Prager Failure Criterion.

Below key steps have been followed for this calculation. However, from Step 1 to 4 are same for all failure criterions. Failure function for respective criterion has been used in Step 5, 6 and 7 separately. The value of critical drawdown pressure P_{CD} (from Step 7) will provide the maximum pressure difference between reservoir pressure and flowing bottom hole pressure that the formation can withstand without sand being produced with the formation fluid.

Step - 1: From a series of formation rock Triaxial tests data, the straight line trend curve is developed using confining pressure and Axial stress. The slope of the trend curve, m and Unconfined Compressive Strength C_0 which is intersection value with Y axis is determined.

In other way, Mohr-Coulomb Failure envelop is developed which is the best fit straight-line tangent that touches maximum number of Mohr circles generated from the Triaxial test data. From the failure envelope equation, the value of Cohesion S_0 and Angle of Internal Friction ϕ has been determined.

Step – 2: From the given reservoir and wellbore information, the in-situ stresses i.e. Vertical/ Overburden Stress σ_V, Maximum Horizontal Stress σ_H and Minimum Horizontal Stress σ_h have been determined.

Step – 3: The Normal Stresses ($\sigma_x, \sigma_y\ and\ \sigma_z$) and Shear Stresses ($\tau_{xy},\ \tau_{yz}$ and τ_{zx}) are calculated at the wellbore coordinate system (Eq. 2-14 to 2-19). The value of β is determined from σ_H azimuth, γ_H and borehole azimuth, γ_w (counterclockwise positive from σ_H direction). (Khalil, Abbas and Toby, 2010)

Step – 4: For sanding application, Θ is the highest stressed point around the wellbore circumference where the Principal Stresses have the highest value. To find out the Θ value, the interval $0 < \Theta < \pi$ has been subdivided into a number of sub-intervals depending on the accuracy required. Using any value of well pressure P_w from 0 to Far field pore pressure P_F, Principal stresses are calculated for each interval. Then Θ is value selected for highest principal stress.

3.1. Mohr-Coulomb Failure Criterion

Step – 5: Using Eq. 2-44, iteration of well pressure P_w and Mohr-Coulomb Failure Function F is performed for highest stressed point at the wellbore wall until the failure function F has the closest value to zero for lowest admissible value of P_w. For each iteration, Axial Stress σ_z, Radial Stress σ_r, Hoop Stress σ_θ, Shear stress $\tau_{\theta z}$ and Principal Stresses i.e. $\sigma_1, \sigma_2\ and\ \sigma_3$ have been calculated.

Wellbore Minimum Pressure $P_{w,\ Min}$ is the minimum admissible well pressure P_w for which the failure function F has the closest value of zero at the highest stressed point of wellbore circumference.

Step – 6: Effective Principal Stresses i.e. σ_1', σ_2' and σ_3' have been calculated using Eq. 2-26 for selected wellbore minimum pressure $P_{w,Min}$. Mohr circle has been developed by the value of σ_1' and σ_3' with the Mohr-Coulomb Failure envelope to check whether the well fails or not.

Step – 7: Critical Drawdown Pressure P_{CD} has been calculated subtracting Minimum Wellbore Pressure $P_{W,\ Min}$ from the Far Field Pore pressure P_F using equation 2-34**.**

3.2. Ewy Modified Lade Failure Criterion

Step – 5: Unconfined Compressive Strength C_0 and Modified Lade Friction parameter η has been calculated using Eq. 2-62 and 2-63 respectively.

Step – 6: Using Eq. 2-64, iteration of Well Pressure P_w and Modified Lade Failure Function F is performed for highest stressed point at the wellbore wall until the failure function F has the closest value to zero for lowest admissible value of P_w. For each iteration, Axial Stress σ_z, Radial Stress σ_r, Hoop Stress σ_θ, Shear stress $\tau_{\theta z}$ and Principal Stresses i.e. $\sigma_1, \sigma_2\ and\ \sigma_3$, Modified First Stress Invariant $I_1^{''}$ and Third Stress Invariant $I_3^{''}$ have been calculated.

Wellbore Minimum Pressure $P_{w,\ Min}$ is the minimum admissible well pressure P_w for which the failure function F has the closest value of zero at the highest stressed point of wellbore circumference.

Step – 7: Critical Drawdown Pressure P_{CD} has been calculated subtracting Minimum Wellbore Pressure $P_{W,\ Min}$ from the Far Field Pore pressure P_F using equation 2-34**.**

3.3. Mogi-Coulomb Failure Criterion

Step – 5: Mogi-Coulomb material constants a and b have been calculated using Eq. 2-56 and 2-57 respectively.

Step – 6: Using Eq. 2-58, iteration of Well pressure P_w and Mogi-Coulomb Failure Function F is performed for highest stressed point at the wellbore wall until the failure function F has the closest value to zero for lowest admissible value of P_w. For each iteration, Axial Stress σ_z, Radial Stress σ_r, Hoop Stress σ_θ, Shear stress $\tau_{\theta z}$ and Principal Stresses i.e. $\sigma_1, \sigma_2\ and\ \sigma_3$, Effective Mean Stress $\sigma'_{m,2}$ and Octahedral Shear Stress τ_{oct} have been calculated.

Wellbore Minimum Pressure $P_{w,\ Min}$ is the minimum admissible well pressure P_w for which the failure function F has the closest value of zero at the highest stressed point of wellbore circumference.

Step – 7: Critical Drawdown Pressure P_{CD} has been calculated subtracting Minimum Wellbore Pressure $P_{W,\ Min}$ from the Far Field Pore pressure P_F using equation 2-34**.**

3.4. Drucker-Prager Failure Criterion

Step – 5: Mogi-Coulomb material constants a and k have been calculated using Eq. 2-40 and 2-51 respectively.

Step – 6: Using Eq. 2-52, iteration of well pressure P_w and Drucker-Prager failure Function F is performed for highest stressed point at the wellbore wall until the failure function F has the closest value to zero for lowest admissible value of P_w. For each iteration, Axial Stress σ_z, Radial Stress σ_r, Hoop Stress σ_θ, Shear stress $\tau_{\theta z}$ and Principal Stresses i.e. $\sigma_1, \sigma_2 \, and \, \sigma_3$, Effective Mean Stress $\sigma'_{m,2}$ and Octahedral Shear Stress τ_{oct} have been calculated.

Wellbore Minimum Pressure $P_{w,\, Min}$ is the minimum admissible well pressure P_w for which the failure function F has the closest value of zero at the highest stressed point of wellbore circumference.

Step – 7: Critical Drawdown Pressure P_{CD} has been calculated subtracting Minimum Wellbore Pressure $P_{W,\, Min}$ from the far field Pore pressure P_F using equation 2-34.

Chapter 4: Case Study

In this case study, Critical Drawdown Pressure has been calculated for predicting sanding potential of a gas well of Bangladesh. Well #A is a deviated well with open hole completion drilled in a sandstone reservoir.

The well is in production and the assumption has been made that:

- Borehole wall is permeable.
- The local pore Pressure at the borehole wall is equal to the wellbore bottom hole flowing pressure ($P_f = P_w$).

The information of reservoir formation and Well #A has been provided in Table 4-1 and Table 4-2 respectively.

Table 4-1: Reservoir and Production Information

Reservoir Depth, H	9437 Feet
Initial Reservoir Pore Pressure at 9437 feet, P_F	4245 psig
Current gas production Rate, V	25 MMSCFD
Bottom Hole Flowing Pressure, BHFP, P_w	2300 psig
Reservoir Lithology	Sandstone
Poisson Ratio, ν	0.2
Final abandon reservoir pressure	200 psig

For study purpose and simplicity, it has been assumed that Well #A formation is homogeneous, linear-Elastic with Biot Poroelastic Constant, k = 1.

Table 4-2: Well information

Well Deviation, α	23^0
Well TVD	11296 Feet
Well MD	12221 Feet
Well Azimuth, γ_w	260^0
Well Completion	Open Hole with no screen and gravel pack arrangement

Table 4-3: Wellbore Stress Information

Vertical Stress Gradient at Reservoir Depth, σ_V	0.944 psi/feet
Minimum Horizontal Stress Gradient at Reservoir Depth, σ_H	0.75 psi/feet
Maximum Horizontal Stress Gradient at Reservoir Depth, σ_h	0.96 psi/feet
Direction of Min. Horizontal stress with Azimuth, γ_h	358^0
Direction of Max. Horizontal stress with Azimuth, γ_H	169^0

From World Stress Map, the Assam location with Latitude = 24.95^0 and Longitude = 92.1^0 has been found closest region of Well #A. Hence, the azimuth of minimum and maximum horizontal stress data of Assam location has been used here.

To evaluate rock strength information i.e. Cohesion S_0, Unconfined Compressive Strength $C_{0,}$ Angle of Internal Friction φ, Core sample of Well #A formation was collected and a Triaxial test was performed. Information of core sample and Triaxial test is given in Table 4-4 and Table 4-5 respectively.

Table 4-4: Core Sample Information

Core Interval Depth, TVD	8639 – 8920 Feet
Number of Core sample for Triaxial Test	6
Length: Diameter of each Core Sample	2:1
Diameter of each Core Sample	0.75 Inch
Length of each Core Sample	1.5 Inch

Table 4-5: Triaxial Test Data for Well #A core

Test Number	Effective Confining Pressure, σ_3'	Effective Peak Strength, σ_1'
Test 1	0	7090
Test 2	306	7904
Test 3	804	11147
Test 4	1508	14161
Test 5	2706	21303
Test 6	4204	25113

4.1.1. Critical Drawdown Pressure Calculation

Step – 1: Using the given Triaxial Test data of Table 4-5, Triaxial Confined Compression result curve in Fig 4-1 has been developed. From the equation of the trend line, Unconfined Compressive Strength, C_0 = 7271 psi.

Slope of the trend curve, m = 4.522

From Eq. 2-39, the Angle of Internal Friction, $\phi = 39.6^0$

From Eq. 2-41, Cohesion C_0 = 1710 psi

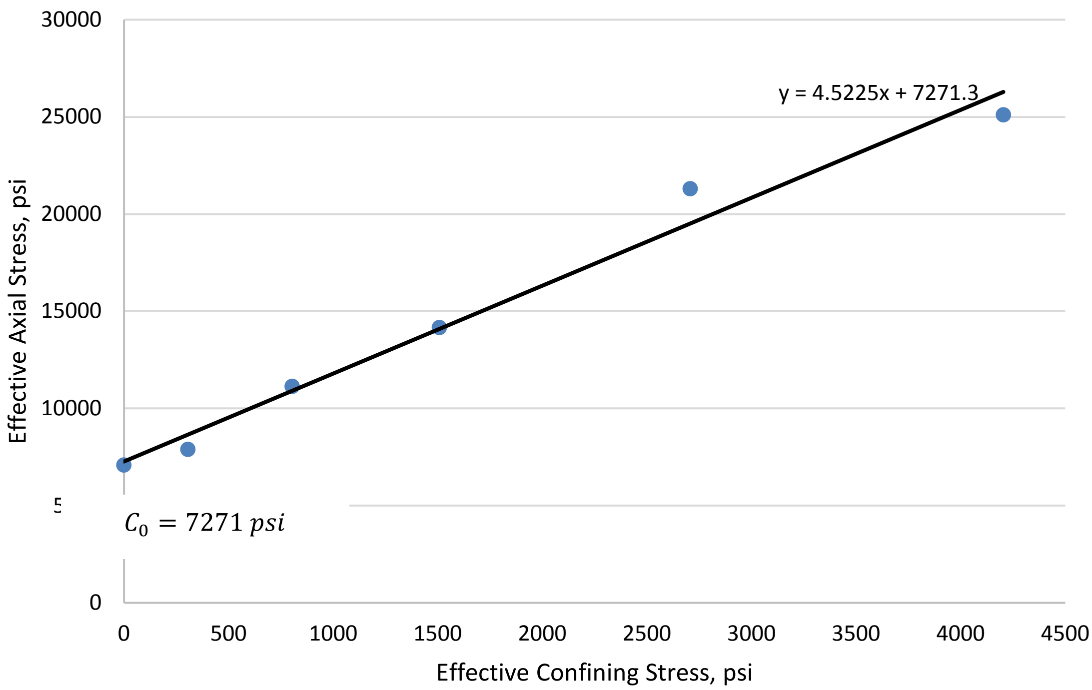

Figure 4-1: Ultimate Axial Stress-Confining Pressure Curve for Well #A

Mohr-Coulomb Failure envelop is the best fit straight-line tangent that touches most of the Mohr circles generated from the Triaxial test data. Using MohrView software, the Mohr Circle and the Failure Envelop has been drawn in Fig, 4-2 using Triaxial Test data, Cohesion S_0 and Angle of Internal Friction ϕ.

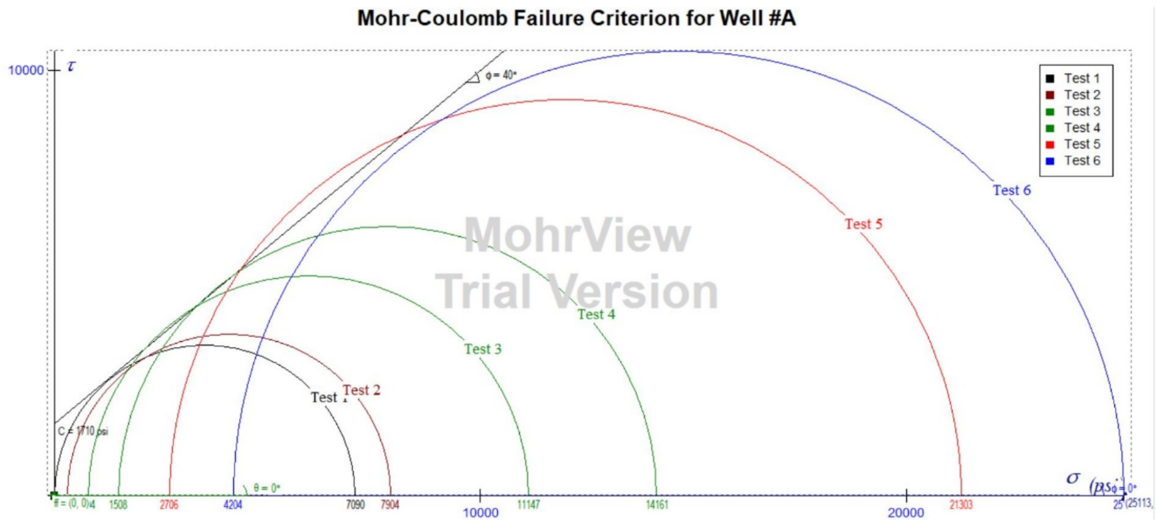

Figure 4-2: Mohr-Coulomb Criterion in τ-σ/ space for Well #A.

Step – 2: In-Situ Stresses at the wellbore wall are calculated directly from the given stress gradient in Table: 4-6.

Table 4-6: In-Situ Stresses at the wellbore wall

Vertical or Overburden Stress, σ_V	8909 psi
Minimum Horizontal Stress, σ_h	7078 psi
Maximum Horizontal Stress, σ_H	9060 psi

Step – 3: In-situ Normal Stresses (σ_x, σ_y and σ_z) and Shear Stresses (τ_{xy}, τ_{yz} and τ_{zx}) in Rectangular Wellbore Coordinate System has been calculated from In-Situ stresses using Eq. 2-14 to Eq. 2-19.

β is the angle between the hole direction (projection on plane) and σ_H direction (counterclockwise positive from σ_H direction). From below figure,

$$\beta = 269^0$$

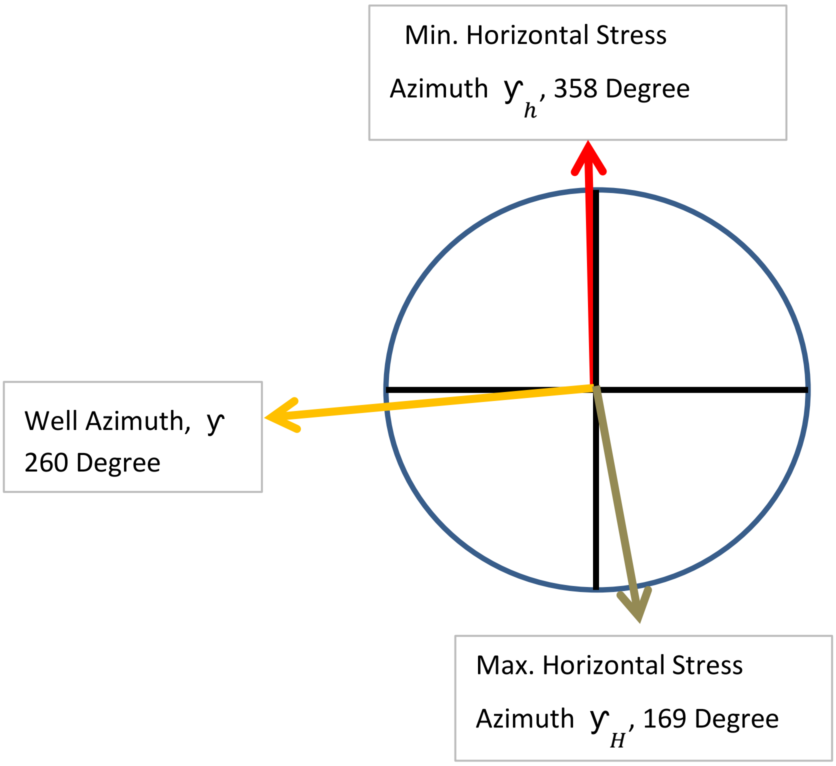

Figure 4-3: Wellbore and Wellbore Minimum/Maximum Stress Azimuth.

Table 4-7: Stresses in Rectangular Wellbore Coordinate System

Normal Stress	σ_x	7358 psi
	σ_y	9059 psi
	σ_{zz}	8629 psi
Shear Stress	τ_{xy}	-32 psi
	τ_z	-658 psi
	τ_{zx}	-14 psi

Step – 4: The interval $0 < \Theta < \pi$ has been subdivided in to a number of sub-intervals of 10^0 value. It has been found that the highest stressed point at the wellbore wall has been found at $\Theta = 0^0$ where the Principal stresses i.e. σ_1, σ_2 and σ_3 have the largest value for any well pressure P_w for 0 to 4245 psi (Pore pressure).

A sample calculation for calculating stresses around wellbore has been shown in Appendix A.

4.1.2. CDP Calculation by Calculation Mohr-Coulomb Failure Criterion

Step – 5: From iteration of F and P_w, it has been found that at highest stressed point of wellbore wall where $\Theta = 0^0$, the Mohr Coulomb Failure Function F = - 4062 for Minimum well pressure P_w = 4245 psi. The Axial Stress σ_z, Radial Stress σ_r, Hoop Stress σ_θ, Shear stress $\tau_{\theta z}$, Principal Stresses (i.e. σ_1, σ_2 and σ_3) and Effective Principal Stresses (i.e. σ_1', σ_2' and σ_3') have been calculated for the same iteration and shown in the below Table.

Table 4-8: Mohr-Coulomb Failure Criterion Calculation

P_w	F (Eq. 2-43)	$\sigma_r = P_w$ (Eq. 2-20)	σ_Θ (Eq. 2-21)	σ_z (Eq. 2-21)	$\tau_{\Theta z}$ (Eq. 2-23)	σ_1 (Eq. 2-26)	σ_2 (Eq. 2-26)	σ_3 (Eq. 2-26)	σ_1' (Eq. 2-31)	σ_2' (Eq. 2-32)	σ_3' (Eq. 2-33)
4255	-4042	4255	15564	9529	-27	15565	9529	4255	11310	5274	0
4220	-4072	4240	15579	9529	-27	15580	9529	4240	11340	5289	0
4245	-4062	4245	15574	9579	-27	15575	9529	4245	11330	5284	0

Step – 6: From the above iteration Table: 4-8, the Mohr-Coulomb Failure Function F = -4062 at the highest stressed point of wellbore #A ($\Theta = 0^0$) when the wellbore pressure is minimum at $P_{w,Min}$ = 4245 psig. It has been seen that $P_{w, Min}$ is same as Pore Pressure P_F. Using Eq. 2-34, the Critical Drawdown pressure P_{CD} is 0 psi for $P_{w,Min}$ = 4245 at $\Theta = 0^0$.

So, Mohr-Coulomb Model predicts that sand will start producing even when flowing bottom hole pressure is equal to far field reservoir pressure i.e. drawdown is zero.

A sample calculation for P_w = 4245 psi has been shown in Appendix B.

Mohr-Coulomb Circle for Well #A at P_w = 4245 psig with Failure Envelope has been drawn with the effective principal stresses in Fig. 4-4.

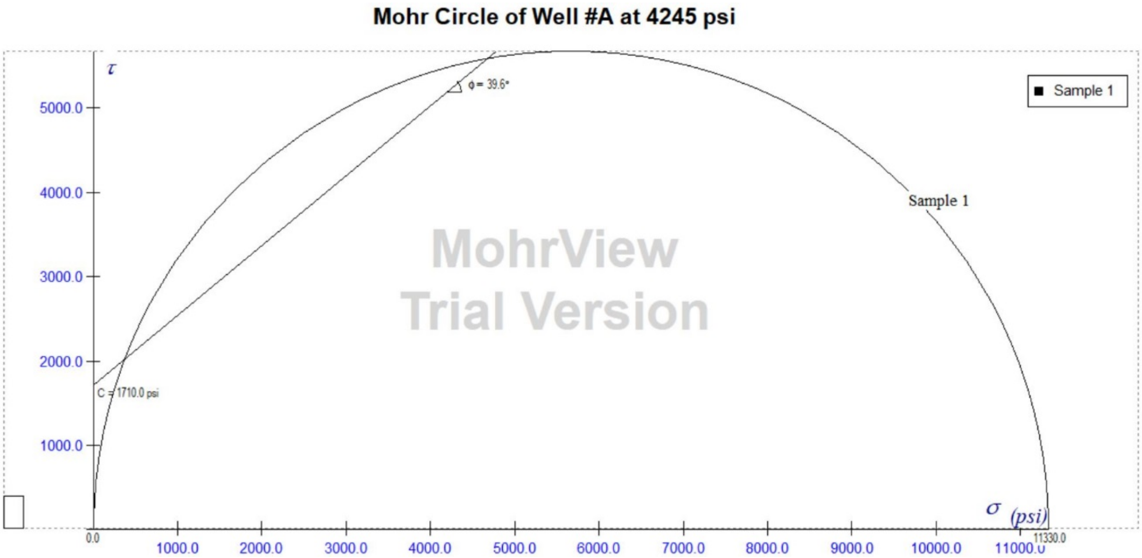

Figure 4-4: Mohr-Coulomb Circle for Well #A with Failure Envelope

4.1.3. CDP Calculation by Modified Lade Criterion

From Eq. 2-62, Unconfined Compressive Strength $C_0 = \frac{S_0}{tan\phi}$ = 2067 psi

From Eq. 2-63, Modified Lade Friction parameter $\eta = \frac{4\,tan^2\phi\,(9-7\,sin\phi)}{(1-sin\phi)}$= 34

From iteration of F and P_w, it has been found that at highest stressed point of wellbore wall where $\Theta = 0^0$, the Modified Lade Failure Function F = 0 for minimum well pressure P_w = 3561 psi. The Axial Stress σ_z, Radial Stress σ_r, Hoop Stress σ_Θ, Shear stress $\tau_{\Theta z}$, Principal Stresses i.e. σ_1, σ_2, $\sigma_3$and Modified Lade First Stress Invariant I_1, Third Stress Invariant I_3 have been calculated for the same iteration and shown in the below Table.

Table 4-9: Modified Lade Failure Criterion Calculation

P_w	F (Eq. 2-62)	$\sigma_r = P_w$ (Eq. 2-20)	σ_Θ (Eq. 2-21)	σ_z (Eq. 2-21)	$\tau_{\Theta z}$ (Eq. 2-23)	σ_1 (Eq. 2-26)	σ_2 (Eq. 2-26)	σ_3 (Eq. 2-26)	I_1'' (Eq. 2-58)	I_3'' (Eq. 2-59)
3570	0.04	3570	15817	9529	-27	15817	9529	3570	24408	$2.37x10^{11}$
3550	-0.05	3550	15824	9529	-27	15824	9529	3550	24455	$2.38x\,10^{11}$
3561	0	3561	15820	9529	-27	15821	9529	3561	24429	$2.38x\,10^{11}$

Using Eq. 2-34, the Critical Drawdown pressure P_{CD} is 684 psi for $P_{w,Min}$ = 3561 psi at $\Theta = 0^0$. A sample calculation for P_w = 3561 psi has been shown in Appendix C.

4.1.4. CDP Calculation by Mogi-Coulomb Failure Criterion

From Eq. 2-56, Material Constant $a = \frac{2\sqrt{2}}{3} S_0 cos\phi$ = 1242 psi.

From E. 2-57, Material Constant $b = \frac{2\sqrt{2}}{3}\ sin\phi$ = 0.6

From iteration of F and P_w, it has been found that at highest stressed point of wellbore wall where $\Theta = 0^0$, the Mogi-Coulomb Failure Function F = 0 for minimum well pressure P_w = 4130 psi. The Axial Stress σ_z, Radial Stress σ_r, Hoop Stress σ_Θ, Shear stress $\tau_{\Theta z}$, Principal Stresses i.e. σ_1, σ_2, σ_3, Effective Mean stress $\sigma'_{m,2}$ and Octahedral Shear Stress τ_{oct} have been calculated for the same iteration and shown in the below Table.

Table 4-10: Mogi-Coulomb Failure Criterion Calculation

P_w	F (Eq. 2-56)	$\sigma_r = P_w$ (Eq. 2-20)	σ_Θ (Eq. 2-21)	σ_z (Eq. 2-21)	$\tau_{\Theta z}$ (Eq. 2-23)	σ_1 (Eq. 2-26)	σ_2 (Eq. 2-26)	σ_3 (Eq. 2-26)	σ'_1 (Eq. 2-31)	σ'_2 (Eq. 2-32)	σ'_3 (Eq. 2-33)	$\sigma'_{m,2}$ (Eq. 2-52)	τ_{oct} (Eq. 2-53)
4140	2	4140	15612	9462	-27	15612	9462	4140	11472	5322	0	5736	4688
4120	-1	4120	15619	9449	-27	15620	9449	4120	11500	5329	0	5750	4699
4125	0	4125	15618	9452	-27	15618	9452	4125	11493	5327	0	5746	4696

Using Eq. 2-34, the Critical Drawdown pressure P_{CD} is 120 psi for $P_{w,Min}$ = 4125 psi at $\Theta = 0^0$. A sample calculation for P_w = 4130 psi has been shown in Appendix D.

4.1.5. CDP Calculation by Drucker-Prager Failure Criterion

From Eq. 2-50, Material constant $\alpha = \frac{2sin\phi}{\sqrt{3}(3-sin\phi)}$ = 0.31

From Eq. 2-51, Material Constant $k = \frac{6ccos\phi}{\sqrt{3}(3-sin\phi)}$ = 1932 psi

From iteration of F and P_w, it has been found that at highest stressed point of wellbore wall where $\Theta = 0^0$, the Drucker-Prager Failure Function F = 0 for minimum well pressure P_w = 0 psi. The Axial Stress σ_z, Radial Stress σ_r, Hoop Stress σ_θ, Shear stress $\tau_{\theta z}$, Principal Stresses i.e. σ_1, σ_2 *and* σ_3 First Stress Invariant I_1 and the Second Deviatoric Stress Invariant J_2 have been calculated for the same iteration and shown in the below Table.

Table 4-11: Drucker-Prager Failure Criterion Calculation

P_w	F (Eq. 2-49)	$\sigma_r = P_w$ (Eq. 2-20)	σ_Θ (Eq. 2-21)	σ_z (Eq. 2-21)	$\tau_{\Theta z}$ (Eq. 2-23)	σ_1 (Eq. 2-26)	σ_2 (Eq. 2-26)	σ_3 (Eq. 2-26)	σ_1' (Eq. 2-31)	σ_2' (Eq. 2-32)	σ_3' (Eq. 2-33)	I_1 (Eq. 2-45)	J_2 (Eq. 2-46)
10	774	10	17097	6817	-27	17097	6817	10	17087	6807	0	23895	7.4×10^7
5	773	5	17099	6814	-27	17099	6814	5	17094	6809	0	23903	7.4×10^7
0	772	0	17101	6811	-27	171001	6811	0	17101	6811	0	23912	7.4×10^7

Using Eq. 2-34, the Critical Drawdown pressure P_{CD} is 4245 psi for $P_{w,Min} = 0$ at $\Theta = 0^0$.

A sample calculation for P_w = 0 psi has been shown in Appendix E.

Chapter 5: Observations and Discussions

Summary of the sanding potentiality evaluation of Well #A by Mohr-Coulomb, Mogi-Coulomb, Modified Lade and Drucker-Prager failure criterions are given in Table 5-1:

Table 5-1: Summary Result Sanding Potentiality Evaluation of Well #A

Failure Criterion	**Minimum Well Pressure $P_{w,Min}$**	**Failure Function, F**	**Critical Drawdown, P_{CD}**
Mohr-Coulomb	4245	-2521	0
Mogi-Coulomb	4125	0	120
Modified Lade	3561	0	684
Drucker-Prager	0	772	4245

From Step 4, it has been found that the $\theta = 0^0$ value for highest stressed point at the wellbore circumference is same for all four models. If the wellbore is vertical, θ equals to zero. If the wellbore is deviated, θ value largely depends on the wellbore deviation α, azimuth β and wellbore stress.

Figure 4-2 Mohr-Coulomb Circle for Well #A with Failure Envelope indicates that Well #A will fail and sand production will commence as soon as the well is in production. At highest stressed point of the wellbore circumference $\theta = 0^0$, the Failure Function F = -4062 which is far away from F = 0 and Wellbore pressure equals to Far-field Pore pressure $P_W = P_f$ = 4245 psi. To make F = 0, the well pressure P_w needs to be increase above 4245 psi which is not possible because the reservoir pore pressure P_F is 4245 psi. Mohr-Coulomb failure criterion predicts that Well #A will produce sand as soon as gas production will be started.

Currently Well #A is in production with 25 MMSCFD gas flow rate at well pressure 2300 psig pressure. Although there is no indication of sand production at the current production rate, but according to Mohr-Coulomb Failure criterion, the well is supposed to produce sand at current production rate. So it can be said that, Mohr-Coulomb Failure criterion is a very conservative failure model which does not consider the strengthening effect of Intermediate stress. Additionally, Mohr-Coulomb failure criterion is based on the assumption that the shear stress τ is a linear function of normal stress σ'(Fjaer et.al. 2008. P. 84). But in reality, the actual rock behavior is non-linear and hence there will be some inaccuracy.

Mogi-Coulomb Criterion considers the strengthening effect of Intermediate stress and predicts that the well formation rock will not fail at its highest stressed point until the well pressure drops below 4125 psi. Hence the critical drawdown pressure is 120 psi. So according to this Criterion Well #A has capability to produce very little amount of gas without producing sand until the Critical Drawdown pressure P_{CD} = 120 psi.

As like as Mogi-Coulomb failure criterion, the Modified Lade failure criterion also considers the strengthening effect of the intermediate stress σ_2. This failure criterion shows that the Well #A will start producing sand when the well pressure P_w drops below 3561 psi or Critical Drawdown pressure P_{CD} is higher than 684 psi.

Mogi-Coulomb and Modified Lade failure criterion are moderate conservative method to predict the rock strength for sanding application. Both criterions predict that the gas production can be increased from Well #A. According to Modified Lade Criterion and Mogi-Coulomb failure criterion, the Minimum Well Pressure $P_{w,Min}$ can be 3561 psi and 4125 psi respectively without any potential sand production. However, the current gas production from Well #A is 25 MMSCFD at 2300 psig bottom hole well pressure which is lower than predicted minimum well pressure by Modified Lade and Mogi-Coulomb failure criterion.

According to Drucker-Prager Failure criterion, the Failure function F is always greater than zero and Well #A will not fail during its entire production lifetime at full opening of well choke valve. Drucker-Prager failure criterion predicts that Well #A can produce 85 MMSCFD (Choke valve maximum capacity at full opening is 85 MMSCFD) gas without any sand production. Although Drucker-Prager failure criterion overestimates the strengthening effect of the Intermediate Stress and hence the least conservative sand production model, the result of this model explains why the well is still producing gas

(25 MMSCFD) at lower bottom hole well pressure (2300 psig) without any sand production.

The Drucker–Prager failure criterion is easy to use and implement in numerical models, but due to the potentially large errors that can occur in estimating intact rock strength, its use should be limited to a narrow range of stresses in the vicinity of the intermediate and minor principal stresses from which the parameters of the criterion are obtained. (Alejano and Bobet. 2012).

Chapter 6: Conclusions and Recommendations

From the above observation and discussion, following conclusions have been made:

- The result of sanding potentiality analysis confirms that Mohr-Coulomb Failure criterion is most conservative failure model; Modified Lade and Mogi-Coulomb failure criterion is moderate and Drucker-Prager Failure criterion is the least conservative failure model. This result is aligned with other sanding potentiality prediction work done by Ewy 1999, Al – Ajmi and Zimmerman 2006.
- From the result of formation rock failure criterions, it can be concluded that Mohr-Coulomb, Mogi-Coulomb and Modified Lade failure criterions are not good for sand production prediction with drawdown (underbalance situation). These are good for wellbore stability analysis with slight overbalance for drilling operation. Only Drucker Prager failure criterion results matches with current Well #A operating condition and hence can be considered as a reliable criterion for underbalance condition.

From the above conclusions following recommendations have been made for Well #A:

- Finite Element Method (FEM) can be applied for more reliable prediction on sanding potentiality of Well #A. The inaccuracy related with linear function of Shear Stress τ and Normal Stress σ' of Mohr-Coulomb Failure criterion can be overcome by employing non-linear FEM. In such model, the actual non-linear behavior of the rock and its path-dependent interactions with the surrounding rock and stresses are accounted for. As a result, predictions from carefully performed FEM can be quite reliable. However, this approach is more time consuming and requires rigorous data input and modeling (Ewy et. al. 1990).
- As it is pretty obvious from Drucker-Prager failure criterion that gas can be produced at higher rate from Well #A, efforts can be made to increase production rate on an experimental basis. At each step of increased production rate and reduced well pressure P_w, the presence of sand with the incoming fluid must be checked and analyzed very carefully. As soon as sand is found with the incoming fluid, production rate shall be hold at this point.

- If sand production triggers due to increased gas production, some sand control measures can be applied i.e. screen installation without gravel pack, gravel pack without screen or gravel pack with screen etc. However, all these sand control techniques will reduce the production index at various degree depending on the taken measures. To increase gas production, well pressure needs to be reduced sufficiently by opening the Choke valve.
- On the process facility, proper sand monitoring facility i.e. sand probe etc. needs to be installed and regular preventive maintenance needs to be carried out to make sure that the system is providing reliable data of the presence of sand.
- If sand is coming to the facility side, sand catcher or other remedial actions can be installed to collect those sands before it reaches to the facility and damage the equipment.

References

Al-Ajmi, A.M., Sultan Qaboos U.: and Zimmerman, R.W. 2006. Stability analysis of deviated boreholes using the Mogi-Coulomb failure criterion, with applications to some oil and gas reservoirs. SPE 104035 presented at IADC/SPE Asia Pacific Drilling Technology Conference and Exhibition, Bangkok, Thailand, 13-15 November, 2006.

Alejano Leandro R. and Bobet Antonio. 2012. Drucker-Prager Criterion. Article in Rock Mechanics and Rock Engineering, November 2012 45:995-999

Ewy R.T. Wellbore-Stability Predictions by use of a Modified Lade Criterion. SPE 56862 published in SPE Drill & Completion, Vol 14, No. 2, June 1999

Ewy R.T., Ray P., Bovberg C.A., Norman P.D. and Goodman H. E. Openhole Stability and Sanding Predictions by 3D Extrapolation from Hole Collapse Tests. SPE 56592 presented at SPE Annual Technical Conference and Exhibition, Texas 3-6 October, 1999.

Fjaer E., Holt R.M., Horsrud P., Raeen A.M. and Risnes R. 2008 Petroleum Related Rock Mechanics 2nd Edition, Elsevier, Boulevard, Langford Lane, Kidlington, UK.

ImmersteinTonje. 2013 Wellbore Stability and Rock Mechanics Study on the Ula field. Master’s Thesis, Faculty of Science and Technology, University of Stavanger, Norway

McLean M. R. and Addis M. A. Wellbore Stability: The Effect of Strength Criteria on Mud Weight Recommendations. SPE 20405 presented at the 65th SPE Annual Technical Conference and Exhibition, New Orleans, LA, September 23-26, 1990.

Zhang Lianyang, Cao Pig and Radha K.C. 2010.Evaluation of rock strength for wellbore stability analysis. International Journal of Rock Mechanics & Mining Sciences 47 (2010) 1304-1316.

Khalil Rahman, Abbas Khaksar and Toby Kayes: An integrated geomechanical and passive sand-control approach to minimizing sanding risk from Openhole and cased-and- perforated wells. SPE-116633-PA, 2010.

World Stress Map Database Released 2016. Downloaded 04 August, 2017. http://dataservices.gfz-potsdam.de/wsm/showshort.php?id=escidoc:1680890

MohrView Mohr-Coulomb Plotting and Analysis. Downloaded 29 October, 2017 http://www.scisoftware.com/environmental_software/product_info.php?products_id=150

Appendix - A

Stresses around Wellbore #A calculation (Step 2 – 4)

Step 2-4 as mentioned in the Outlined Methodology is applicable for all four failure criterions.

In-Situ Stresses of Well #A

Given,

Stresses to be calculated at H = 9437 Feet depth of Well #A.

As per Stress Gradient of Table 4-3,

Vertical or Overburden Stress, σ_v = 9437 x 0.944 = 8909 psi

Minimum Horizontal Stress, σ_h = 9437 x 0.75 = 7078 psi

Maximum Horizontal Stress, σ_H = 9437 x 0.96 = 9060 psi

Stresses in Wellbore Coordinate System

Given,

Wellbore Azimuth γ_w = 260^0

Wellbore Deviation/Inclination α = 23.3^0

From World Stress Map for Latitude = 24.95^0 and Longitude = 92.1^0,

Azimuth of Maximum Horizontal Stress, γ_H = 169^0

Angle between γ_w and γ_H (counterclockwise positive γ_H), β = 269^0

Eq. (2-14) Normal Stress in X-Direction,

$$\sigma_x \quad = \sigma_H sin^2\beta + \sigma_h cos^2\beta$$

$= 9060 \times (\sin 269^0)^2 + 7078 \times (\cos 269^0)^2$

$= 7358$ psi

Eq. (2-15) Normal Stress in Y-Direction,

$$\sigma_y = \cos^2\alpha(\sigma_H \cos^2\beta + \sigma_h \sin^2\beta) + \sigma_V \sin^2\alpha$$

$= (\cos 23^0)^2 \times \{9060 \times (\cos 269^0)^2 + 7078 \times (\sin 269^0)^2\} + 8909 \times (\sin 23^0)^2$

$= 9059$ psi

Eq. (2-16) Normal Stress along wellbore axial Direction,

$$\sigma_{zz} = \sin^2\alpha \begin{pmatrix} \sigma_H \cos^2\beta + \\ \sigma_h \sin^2\beta \end{pmatrix} + \sigma_V \cos^2\alpha$$

$= (\sin 23^0)^2 \times \{9060 \times (\cos 269^0)^2 + 7078 \times (\sin 269^0)^2\} + 8909 \times (\cos 23^0)^2$

$= 8629$ psi

Shear Stresses,

Eq. (2-17), $\tau_{xy} = \cos\alpha \sin\beta \cos\beta(\sigma_H - \sigma_h)$

$= \cos 23^0 \times \sin 269^0 \times \cos 269^0 \times (9060 - 7078)$

$= -32$ psi

Eq. (2-18), $\tau_{yz} = \sin\alpha \cos\alpha(\sigma_V - \sigma_H \cos^2\beta - \sigma_h \sin^2\beta)$

$= \sin 23^0 \times \cos 23^0 \times (8909 – 9060 \times \cos^2 269^0 – 7078 \times \sin^2 269^0)$

$= -14$ psi

Eq. (2-19), $\tau_{zx} = \sin\alpha \sin\beta \cos\beta(\sigma_h - \sigma_H)$

$= \sin 23^0 \times \sin 269^0 \cos 269^0 \times (7078 - 9060) = -658$ psi

Appendix - B

CDP calculation by Mohr-Coulomb Failure Criterion

For different value of Well Pressure P_w the Mohr Coulomb Failure Function F has been calculated. This iteration has been done at the highest stressed point of wellbore wall until the failure function F has the closest value to zero for lowest admissible value of P_w.

Here only one calculation for P_w = 4245 psi has been shown for example:

Given,

Reservoir Far field Pore Pressure P_F = 4245 psi

Highest Stressed Point at wellbore wall is at $\Theta = 0^0$

Poisson ratio ν = 0.265

Biot Poroelastic Coefficient, k = 1

Poroelastic Stress Coefficient, $\alpha_0 = k\,\frac{(1-2v)}{(1-\nu)}$ = $\frac{1*(1-2*0.265)}{(1-0.265)}$= 0.64

From Triaxial Test Result,

Cohesion, S_0 = 1710 psi

Angle of Internal Friction, $\varphi = 39.6^0$

From Eq. 2-20, Radial Stress, σ_r = P_w = 4245 psi

From Eq. 2-22, Hoop Stress,

$$\sigma_\theta = \sigma_x + \sigma_y - 2(\sigma_x - \sigma_y)cos2\theta - 4\tau_{xy}sin2\theta - P_w + \alpha_0(P_w - P_F)$$

= 7358 + 9059 – 2 x (7358 – 9059) x cos(2 x 0^0) – 4 x (-32) x sin(2 x 0^0) – 4245 + 0.64 x (4245 – 4245) = 15574 psi

From Eq. 2-22, Axial Stress,

$$\sigma_z = \sigma_{zz} - \upsilon\left[2\left(\sigma_x - \sigma_y\right)cos2\theta + 4\tau_{xy}sin2\theta\right] + \alpha_0(P_w - P_F)$$

= 8629 – 0.265 x [2 x (7358 - 9059) x cos(2 x 0^0) + 4 x (-32) x sin(2 x 0^0)] + 0.64 x (4245 - 4245)

= 9529 psi

From Eq. 2-23, Shear Stress,

$$\tau_{\theta z} = 2(\tau_{yz}cos\theta - \tau_{zx}sin\theta)$$

= 2 x [(-14) x cos 0^0 – (-658) sin 0^0]

= - 27 psi

From Eq. 2-26, Principal Stresses,

$$\sigma_1, \sigma_2, \sigma_3 = \begin{cases} \frac{\sigma_\theta + \sigma_z}{2} + \sqrt{[(\frac{\sigma_\theta - \sigma_z}{2})^2 + \tau_{\theta z}^2]} \\ \frac{\sigma_\theta + \sigma_z}{2} - \sqrt{[(\frac{\sigma_\theta - \sigma_z}{2})^2 + \tau_{\theta z}^2} \\ P_w \end{cases}$$

$$\sigma_1 = \frac{\sigma_\theta + \sigma_z}{2} + \sqrt{[(\frac{\sigma_\theta - \sigma_z}{2})^2 + \tau_{\theta z}^2]}$$

$$= \frac{15574 + 9529}{2} + \sqrt{[(\frac{15574 - 9529}{2})^2 + (-27)^2]}$$

$= 15575$ psi

$$\sigma_2 = \frac{\sigma_\theta + \sigma_z}{2} - \sqrt{[(\frac{\sigma_\theta - \sigma_z}{2})^2 + \tau_{\theta z}^2]}$$

$$= \frac{15574 + 9529}{2} - \sqrt{[(\frac{15574 - 9529}{2})^2 + (-27)^2]}$$

$$= 9529 \text{ psi}$$

σ_3 = P_w = 4245 psi

From Eq. 2-31, 2-32 and 2-33, Effective Principal Stresses are –

$$\sigma_1' = 15575 - 4245 = 11330\, psi$$

$$\sigma_2' = 9529 - 4245 = 5284\, psi$$

$$\sigma_3' = 4245 - 4245 = 0\, psi$$

From Eq. 2-45, Moh'r Coulomb Failure Criterion at P_w = 4245 psi

$$F = 2S_0 \frac{cos\phi}{1 - sin\phi} + \sigma_3' \frac{1 + sin\phi}{1 - sin\phi} - \sigma_1'$$

$$= 2 \times 1710 \times \frac{\cos 39.6^0}{1 - \sin 39.6^0} + 0 \times \frac{1 + \sin 39.6^0}{1 - \sin 39.6^0} - 11330$$

= - 4062

From Eq. 2-34, the Critical Drawdown P_{CD} = P_w - $P_{w,Min}$

= 4245 – 4245

= 0

Appendix - C

CDP calculation by Modified Lade Failure Criterion

For different values of Well Pressure P_w the Modified Lade Failure Function F has been calculated. This iteration has been done at the highest stressed point of wellbore wall until the failure function F has the closest value to zero for lowest admissible value of P_w.

Here only one calculation for P_w = 3561 psi has been shown for example:

Given,

Reservoir Far field Pore Pressure P_F = 4245 psi

Highest Stressed Point at wellbore wall is at $\Theta = 0^0$

Poisson ratio ν = 0.265

Biot Poroelastic Coefficient, k = 1

Poroelastic Stress Coefficient, $\alpha_0 = k\,\frac{(1-2\upsilon)}{(1-\nu)} = \frac{1*(1-2*0.265)}{(1-0.265)} = 0.64$

From Triaxial Test Result,

Cohesion, S_0 = 1710 psi

Angle of Internal Friction, $\varphi = 39.6^0$

From Eq. 2-62, Unconfined Compressive Strength, $C_0 = \frac{S_0}{tan\phi}$

$$= \frac{1710}{\tan 39.6^0} = 2067 \text{ psi}$$

From Eq. 2-63, Modified Lade Friction parameter $\eta = \frac{4\,tan^2\phi\,(9-7\,sin\phi)}{(1-sin\phi)}$

$$= \frac{4\ x\ (\tan 39.6)^2 x\ (\ 9-7\sin 39.6)}{(\ 1-\sin 39.6)}$$

= 34

From Eq. 2-20, Radial Stress, $\sigma_r = P_w$

= 3561 psi

From Eq. 2-22, Hoop Stress,

$$\sigma_\theta = \sigma_x + \sigma_y - 2(\sigma_x - \sigma_y)cos2\theta - 4\tau_{xy}sin2\theta - P_w + \alpha_0(P_w - P_F)$$

= 7358 + 9059 – 2 x (7358 – 9059) x cos(2 x 0^0) – 4 x (-32) x sin(2 x 0^0) – 3561 + 0.64 x (3561 – 4245)

= 15820 psi

From Eq. 2-22, Axial Stress,

$$\sigma_z = \sigma_{zz} - v[2(\sigma_x - \sigma_y)cos2\theta + 4\tau_{xy}sin2\theta] + \alpha_0(P_w - P_F)$$

= 8629 – 0.265 x [2 x (7358 - 9059) x cos(2 x 0^0) + 4 x (-32) x sin(2 x 0^0)] + 0.64 x (3561 - 4245)

= 9529 psi

From Eq. 2-23, Shear Stress,

$$\tau_{\theta z} = 2(\tau_{yz}cos\theta - \tau_{zx}sin\theta)$$

= 2 x [(-14) x cos 0^0 – (-658) sin 0^0]

= - 27 psi

From Eq. 2-26, Principal Stresses,

$$\sigma_1, \sigma_2, \sigma_3 = \frac{\sigma_\theta + \sigma_z}{2} + \sqrt{[(\frac{\sigma_\theta - \sigma_z}{2})^2 + \tau_{\theta z}^2]}$$

$$\frac{\sigma_\theta + \sigma_z}{2} - \sqrt{[(\frac{\sigma_\theta - \sigma_z}{2})^2 + \tau_{\theta z}^2}$$

P_w

$$\sigma_1 = \frac{\sigma_\theta + \sigma_z}{2} + \sqrt{[(\frac{\sigma_\theta - \sigma_z}{2})^2 + \tau_{\theta z}^2]}$$

$$= \frac{15820 + 9529}{2} + \sqrt{[(\frac{15920 - 9529}{2})^2 + (-27)^2]}$$

$$= 15821 \text{ psi}$$

$$\sigma_2 = \frac{\sigma_\theta + \sigma_z}{2} - \sqrt{[(\frac{\sigma_\theta - \sigma_z}{2})^2 + \tau_{\theta z}^2]}$$

$$= \frac{15820 + 9529}{2} - \sqrt{[(\frac{15920 - 9529}{2})^2 + (-27)^2]}$$

$$= 9529 \text{ psi}$$

$\sigma_3 = P_w = 3561$ psi

From Eq. 2-60, Modified First Stress Invariant,

$$I_1'' = (\sigma_1 + S_1 - p_f) + (\sigma_2 + S_1 - p_f) + (\sigma_3 + S_1 - p_f)$$

= (15821 + 2067 – 3561) + (9529 + 2067 – 3561) + (3561 +2067 – 3561)

= 24429

From Eq. 2-61, Modified Third Stress Invariant,

$$I_3'' = (\sigma_1 + S_1 - p_f)\ x\ (\sigma_2 + S_1 - p_f)\ x\ (\sigma_3 + S_1 - p_f)$$

= (15821 + 2067 – 3561) x (9529 + 2067 – 3561) x (3561 +2067 – 3561)

= 2.38×10^{11}

From Eq. 2-64, Modified Lade Failure Criterion,

$$F = (27 + \eta) - \frac{(I_1^{"})^3}{I_3^{"}}$$

$$= (27 + 34) - \frac{(24429)^3}{2.38 \; x \; 10^{11}}$$

$$= 0$$

From Eq. 2-34, the Critical Drawdown $P_{CD} = P_w - P_{w,Min}$

$$= 4225 – 3561$$

$$= 684 \text{ psi}$$

Appendix - D

CDP calculation by Mogi-Coulomb Failure Criterion

For different values of Well Pressure P_w the Mogi-Coulomb Failure Function F has been calculated. This iteration has been done at the highest stressed point of wellbore wall until the failure function F has the closest value to zero for lowest admissible value of P_w.

Here only one calculation for P_w = 4125 psi has been shown for example:

Given,

Reservoir Far field Pore Pressure P_F = 4245 psi

Highest Stressed Point at wellbore wall is at $\Theta = 0^0$

Poisson ratio ν = 0.265

Biot Poroelastic Coefficient, k = 1

Poroelastic Stress Coefficient, $\alpha_0 = k\,\frac{(1-2\upsilon)}{(1-\nu)} = \frac{1*(1-2*0.265)}{(1-0.265)} = 0.64$

From Triaxial Test Result,

Cohesion, S_0 = 1710 psi

Angle of Internal Friction, $\varphi = 39.6^0$

From Eq. 2-56 and 2-57, Material Constant,

$$a = \frac{2\sqrt{2}}{3} S_0 \cos\phi = \frac{2\sqrt{2}}{3}\ x\ 1710\ x\ \cos 39.6^0 = 1242 \text{ psi}$$

$$b = \frac{2\sqrt{2}}{3}\ sin\phi = \frac{2\sqrt{2}}{3} sin\ 39.6^0 = 0.6$$

From Eq. 2-20, Radial Stress, $\sigma_r = P_w$ = 4125 psi

From Eq. 2-22, Hoop Stress,

$$\sigma_\theta = \sigma_x + \sigma_y - 2(\sigma_x - \sigma_y)cos2\theta - 4\tau_{xy}sin2\theta - P_w + \alpha_0(P_w - P_F)$$

= 7358 + 9059 – 2 x (7358 – 9059) x cos(2 x 0^0) – 4 x (-32) x sin(2 x 0^0) – 4125 + 0.64 x (4125 – 4245)

= 15618 psi

From Eq. 2-22, Axial Stress,

$$\sigma_z = \sigma_{zz} - \upsilon[2(\sigma_x - \sigma_y)cos2\theta + 4\tau_{xy}sin2\theta] + \alpha_0(P_w - P_F)$$

= 8629 – 0.265 x [2 x (7358 - 9059) x cos(2 x 0^0) + 4 x (-32) x sin(2 x 0^0)] + 0.64 x (4125 - 4245)

= 9452 psi

From Eq. 2-23, Shear Stress,

$$\tau_{\theta z} = 2(\tau_{yz}cos\theta - \tau_{zx}sin\theta)$$

= 2 x [(-14) x cos 0^0 – (-658) sin 0^0]

= - 27 psi

From Eq. 2-26, Principal Stresses,

$$\sigma_1, \sigma_2, \sigma_3 = \begin{cases} \frac{\sigma_\theta + \sigma_z}{2} + \sqrt{[(\frac{\sigma_\theta - \sigma_z}{2})^2 + \tau_{\theta z}^2]} \\ \frac{\sigma_\theta + \sigma_z}{2} - \sqrt{[(\frac{\sigma_\theta - \sigma_z}{2})^2 + \tau_{\theta z}^2]} \\ P_w \end{cases}$$

$$\sigma_1 = \frac{\sigma_\theta + \sigma_z}{2} + \sqrt{[(\frac{\sigma_\theta - \sigma_z}{2})^2 + \tau_z^2]}$$

$$= \frac{15618 + 9452}{2} + \sqrt{[(\frac{15618 - 9452}{2})^2 + (-27)^2]}$$

$= 15618$ psi

$$\sigma_2 = \frac{\sigma_\theta + \sigma_z}{2} - \sqrt{[(\frac{\sigma_\theta - \sigma_z}{2})^2 + \tau_{\theta z}^2]}$$

$$= \frac{15618 + 9452}{2} - \sqrt{[(\frac{15618 - 9452}{2})^2 + (-27)^2]}$$

$= 9452$ psi

$\sigma_3 = P_w = 4125$ psi

From Eq. 2-31, 2-32 and 2-33, Effective Principal Stresses are –

$$\sigma_1' = 15618 - 4125 = 11493\, psi$$

$$\sigma_2' = 9452 - 4125 = 5327\, psi$$

$$\sigma_3' = 4125 - 4125 = 0\, psi$$

From Eq. 2-54, Effective Mean Stress, $\sigma_{m,2}' = \frac{\sigma_1' + \sigma_3'}{2}$= (11493 + 0) / 2 = 5746 psi

From Eq. 2-55, Octahedral Shear Stress,

$$\tau_{oct} = \frac{1}{3}\sqrt{(\sigma_1' - \sigma_2')^2 + (\sigma_2' - \sigma_3')^2 + (\sigma_3' - \sigma_1')^2}$$

$$= \frac{1}{3}\sqrt{(11493 - 5327)^2 + (5327 - 0)^2 + (0 - 11493)^2}$$

$= 4696$ psi

From Eq. 2-58, Mogi-Coulomb Failure Criterion,

$$F = a + b\sigma_{m,2}' - \tau_{oct}$$

$= 1242 + 0.6\ x\ 5746 - 4696$

$= 0$

From Eq. 2-34, the Critical Drawdown $P_{CD} = P_w - P_{w,Min}$

$= 4245 – 4125$

$= 120$ psi

Appendix - E

CDP calculation by Drucker-Prager Failure Criterion

For different values of Well Pressure P_w the Drucker-Prager Failure Function F has been calculated. This iteration has been done at the highest stressed point of wellbore wall until the failure function F has the closest value to zero for lowest admissible value of P_w.

Here only one calculation for P_w = 0 psi has been shown for example:

Given,

Reservoir Far field Pore Pressure P_F = 4245 psi

Highest Stressed Point at wellbore wall is at $\Theta = 0^0$

Poisson ratio ν = 0.265

Biot Poroelastic Coefficient, k = 1

Poroelastic Stress Coefficient, $\alpha_0 = k\,\frac{(1-2\upsilon)}{(1-\nu)} = \frac{1*(1-2*0.265)}{(1-0.265)} = 0.64$

From Triaxial Test Result,

Cohesion, S_0 = 1710 psi

Angle of Internal Friction, $\varphi = 39.6^0$

From Eq. 2-50 and 2-51, Material Constant,

$$\alpha = \frac{2sin\phi}{\sqrt{3}(3 - sin\phi)} = \frac{2sin\,39.6^0}{\sqrt{3}(3 - sin\,39.6^0)} = 0.31$$

$$k = \frac{6\,S_0 cos\phi}{\sqrt{3}(3 - sin\phi)} = \frac{6\,x\,1710x\,cos\,39.6^0}{\sqrt{3}(3 - sin\,39.6^0)} = 1932$$

From Eq. 2-20, Radial Stress, $\sigma_r = P_w$ = 0 psi

From Eq. 2-22, Hoop Stress,

$$\sigma_\theta \quad = \sigma_x + \sigma_y - 2(\sigma_x - \sigma_y)cos2\theta - 4\tau_{xy}sin2\theta - P_w + \alpha_0(P_w - P_F)$$

= 7358 + 9059 – 2 x (7358 – 9059) x cos(2 x 0^0) – 4 x (-32) x sin(2 x 0^0) – 0 + 0.64 x (0 – 4245)

= 17101 psi

From Eq. 2-22, Axial Stress,

$$\sigma_z \quad = \sigma_{zz} - \upsilon[2(\sigma_x - \sigma_y)cos2\theta + 4\tau_{xy}sin2\theta] + \alpha_0(P_w - P_F)$$

= 8629 – 0.265 x [2 x (7358 - 9059) x cos(2 x 0^0) + 4 x (-32) x sin(2 x 0^0)] + 0.64 x (0 - 4245)

= 6811 psi

From Eq. 2-23, Shear Stress,

$$\tau_{\theta z} \quad = 2(\tau_{yz}cos\theta - \tau_{zx}sin\theta)$$

= 2 x [(-14) x cos 0^0 – (-658) sin 0^0]

= - 27 psi

From Eq. 2-26, Principal Stresses,

$$\sigma_1, \sigma_2, \sigma_3 = \begin{cases} \frac{\sigma_\theta + \sigma_z}{2} + \sqrt{[(\frac{\sigma_\theta - \sigma_z}{2})^2 + \tau_{\theta z}^2]} \\ \frac{\sigma_\theta + \sigma_z}{2} - \sqrt{[(\frac{\sigma_\theta - \sigma_z}{2})^2 + \tau_{\theta z}^2} \\ P_w \end{cases}$$

$$\sigma_1 = \frac{\sigma_\theta + \sigma_z}{2} + \sqrt{[(\frac{\sigma_\theta - \sigma_z}{2})^2 + \tau_{\theta z}^2]}$$

$$= \frac{17101 + 6811}{2} + \sqrt{[(\frac{17101 - 6811}{2})^2 + (-27)^2]} = 17101 \text{ psi}$$

$$\sigma_2 = \frac{\sigma_\theta + \sigma_z}{2} - \sqrt{[(\frac{\sigma_\theta - \sigma_z}{2})^2 + \tau_{\theta z}^2]}$$

$$= \frac{17101 + 6811}{2} - \sqrt{[(\frac{17101 - 6811}{2})^2 + (-27)^2]} = 6811 \text{ psi}$$

σ_3 = P_w = 0 psi

From Eq. 2-31, 2-32 and 2-33, Effective Principal Stresses are –

$\sigma_1' = 17101 - 0 = 17101\, psi$

$\sigma_2' = 6811 - 0 = 6811\, psi$

$\sigma_3' = 0 - 0 = 0\, psi$

From Eq. 2-48, First Stress Invariant, $I_1 = \sigma_1' + \sigma_2' + \sigma_3'$= 17101 + 6811 + 0 = 23912

From Eq. 2-49, Second Deviatoric Stress Invariant, $J_2 = \frac{(\sigma_1' - \sigma_2')^2 + (\sigma_2' - \sigma_3')^2 + (\sigma_3' - \sigma_1')^2}{6}$

$$= \frac{(17101 - 6811)^2 + (6811 - 0)^2 + (0 - 17101)^2}{6}$$

= 74120778

From Eq. 2-52, Drucker-Prager Failure Criterion,

$F \quad = \alpha I_1 + k - \sqrt{J_2}$

= 0.31 x 23912 + 1932 - $\sqrt{74120778}$

= 772

From Eq. 2-34, the Critical Drawdown P_{CD} = P_w - $P_{w,Min}$ = 4245 – 0 = 4245 psi